

Emission characteristics of organic meso/nanowires coupled with dielectric and plasmonic structures

A thesis submitted towards the partial fulfilment of
BS-MS Dual Degree Programme

by

Rohit Chikkaraddy



Indian Institute of Science Education and Research,
Pune

Certificate

I hereby certify that the matter embodied in this thesis entitled “Emission characteristics of organic meso/nanowire coupled with dielectric and plasmonic structures” has been carried out by Mr. Rohit Chikkaraddy at the Indian Institute of Science Education and Research, Pune with the supervision of Dr. G. V. Pavan Kumar during the academic year 2013 -2014 and it has not been submitted elsewhere for the award of any degree or diploma.

Rohit Chikkaraddy
(Student)

Dr. G. V. Pavan Kumar
(Supervisor)

Acknowledgements

This thesis and all research that have done in past one year could not have been done without the help of several individuals and it is my great pleasure to acknowledge these people.

I am extremely grateful to my advisor Dr. G.V. Pavan Kumar for maintaining excellent research ambience in the laboratory and providing freedom in choosing research problems. He has always shown great enthusiasm for my research and patiently helped me whenever I have problems. He always encouraged me and gave me a lot of chance to work on varieties of problem though I always made things complicate.

I am very much thankful to my colleges Arindam and Partha (Senior PhD students). They provided valuable help in troubleshooting problems with optical setups, simulations and fabrication of nanostructures. I thank them for spending valuable time with me for explaining the details of simulation software. A special thanks to Ravi and Danveer for helping with capturing FE-SEM images and two-photon images of various samples. A warm thanks to Aswathy for helping me with coupling of organic nanowire with plasmons. I express my gratitude to Adarsh and Sreeja for distracting and taking me for a coffee every now and then.

I would like to thank my friends – Akash, Bhavesh, Aashay and Aditi for providing great motivation.

Abstract

Is it possible to effectively transport light through the channels smaller than the wavelength of light? This is the question that we are trying to answer in this thesis, apparently question is at the heart of nanophotonics. Here we address this issue by harvesting organic meso/nanowires to propagate light from one point to another. In the context of building nanophotonic circuits it is very important to have control over the characteristics of light such as modulation of amplitude, phase and polarization states of light. This is possible via formation of precise junctions and interconnections. Motivated by this we have interfaced organic mesowires with different substrates such as optical cavities and plasmonic films.

Nanophotonic systems such as optical cavities and waveguides have emerged as high sensitive bio-sensors and effective medium for signal transportation, respectively. But fabricating both optical cavities and waveguides in a single architecture is of great challenge and has importance in doing remote detection studies, which has relevance in monitoring photo-physics of light sensitive systems. We interfaced organic mesowires with spherical high-Q microcavity for above mentioned purpose. Further we excite and detect microcavity modes remotely through organic mesowire as a channel of signal transporter. We also observed mode mixing and splitting property of spherical microcavity due to broken azimuthal symmetry. It is very exciting to observe transition in radiation properties from dipolar in simple organic mesowire compared to quadruple in organic mesowire coupled with spherical microcavity.

What are the polarization states of light emitted through the nanowire? How to convert linearly polarized states of light into elliptically polarized light at nanoscale? Addressing these questions has importance in probing chiral molecules at single copy limit and building optical-magnetic recording devices. We have ventured these new polarized states of light in vertical organic nanowires coupled with plasmonic films. These nanowires are standing perpendicular to the substrate, the emission of light from the tip of these nanowire is analysed. These nanowires are excited through energy transport from plasmons to excitons at junctions of metal film and organic nanowire. The emitted light contains elliptically polarized states of light with relatively high degree of polarization 0.41 ± 0.03 ;

Table of Contents

1	<u>Introduction</u>	01
1.1	<u>Optical microcavities</u>	02
1.2	<u>Optical waveguide</u>	04
1.2.1	<u>Surface plasmon polaritons</u>	05
1.2.2	<u>Exciton polaritons</u>	07
2	<u>Growth and wavelength dependent waveguiding properties of Organic Meso/naowire</u>	09
2.1	<u>Growth of organic mesowires</u>	10
2.2	<u>Light propagation (exciton polaritons)</u>	12
2.3	<u>Wavelength dependent light propagation</u>	14
2.4	<u>Directional emission (optical antenna)</u>	15
3	<u>Microsphere coupled organic mesowire: Remote detection of whispering gallery modes</u>	19
3.1	<u>Fabrication of microsphere coupled organic mesowire</u>	21
3.2	<u>Whispering gallery modes</u>	23
3.3	<u>Microsphere coupled organic mesowire</u>	24
3.4	<u>Kramer's degeneracy</u>	26
3.5	<u>Radiation pattern</u>	27
3.6	<u>Conclusion</u>	28

4	<u>Plasmon coupled vertical organic nanowire</u>	29
4.1	<u>Growth of organic vertical nanowire</u>	32
4.2	<u>Optical excitation setup</u>	33
4.3	<u>Emission properties of vertical nanowire</u>	34
4.4	<u>Polarization states of emitted light</u>	36
4.4.1	<u>Probing linearly polarized state of light</u>	36
4.4.2	<u>Probing elliptically polarized state of light</u>	37
4.5	<u>Conclusion</u>	38
5	<u>Future Direction</u>	39
5.1	<u>Exciton coupled with periodic plasmonic tips</u>	39
5.2	<u>Strong coupling between plasmons and excitons</u>	40
6	<u>Appendix</u>	43
	<u>Mie theory</u>	43
7	<u>References</u>	47

Chapter 1

Introduction

Light is the most fascinating spectrum of electromagnetic radiation. This is mainly because energy of light (photon's energy, $E = h \nu$) lies in the electronic transition window of matter¹. Even though light manifests in a form of both waves and particles, often wave picture is used to describe optical radiations and solution to Maxwell's equation provide quantitative picture to the optical phenomenon^{2,3}. Whereas the building blocks of matter (atoms, molecules, quantum dots) with which light interact needs quantum description. In terms of spatial dimensions, light cannot be focused to dimensions smaller than roughly one half of its wavelength (Abbe diffraction limit; $d = \lambda / 2(n \sin\theta)$, where λ is wavelength of light, θ is convergence angle and n is refractive index)⁴, whereas as matters have a spatial dimensions much smaller than the wavelength of light i.e. around 10Å to few nanometres.

Effective interaction of light with matter is hindered due to two orders of magnitude difference in their spatial dimension. However, many natural processes such as photosynthesis effectively harness light energy by utilizing antenna effect to pass energy to the reaction centre through clusters of organic complexes^{5,6}. Thus it is inferred that having a mediator (spatial dimensions around tens of nanometre) to bridge the gap between the dimensions of light and matter can enhance their interaction. Interaction of mediators with light itself has gained tremendous attention recently, due to the technological advancement in fabricating such verities of structures. A new field of nanoscience has emerged dedicated to the study the properties of structures of nanometre dimensions⁷. Nanostructures can be made of metallic, inorganic, organic or polymers, all of them have their own unique properties, but in the context of optics, nanostructures made of metallic and organic have gained significant interest in recent time.

Historically optical experiments revolutionised science in general. Experiments such as black body radiation⁸ and photoelectric effect^{9,10} played an important role in nurturing quantum mechanics. Telescopes and microscopes used to investigate large celestial objects and magnify microorganisms, respectively. As you can see scales from few microns to terrestrial

lengths objects have been imaged through microscopes or telescopes. But scales below the wavelength of light were been unexplored. Nanostructures have opened-up this hidden region and provided access to image objects much smaller than microns in size. Thus the field aiming to understand optical phenomenon on nanometre scale is termed as nano-optics¹¹.

Herein I will introduce to the two important questions of nano-optics on which the entire thesis depends. 1) How to confine light below diffraction limit? 2) How to propagate the light through the channels much smaller than the wavelength of light? Structures that confine the light are termed as cavities and structures that propagate the light are termed as waveguides.

1.1. Optical Microcavities

Resonant recirculation of light in optical microcavities confines the light to small volumes¹². An ideal cavity traps light infinitely (without any losses) and would have sharp resonance frequencies (full width half maxima, FWHM = 0). Deviation from the ideal condition is described by a cavity Q factor. Cavities with larger Q factor confines light for longer time and vice versa. Another factor that is important in the context of miniaturizing optical devices is physical dimension of cavity itself. Cavities with very small volumes and high Q factor are important to realize some fundamental concepts of quantum electro dynamics^{13,14}.

Optical elements such as atoms, molecules or quantum dots placed in a cavity will interaction with the cavity resonances¹⁵. Modified photon density of states in the cavity alters the spontaneous decay process of the optical elements¹³. Historically, Purcell¹⁶ discovered the enhancement of spontaneous emission rates of atoms when they are matched in a resonant cavity (the Purcell Effect). The enhancement is given by the Purcell factor¹³

$$F_p = \frac{3}{4\pi^2} \left(\frac{\lambda_c}{n}\right)^3 \left(\frac{Q}{v}\right) \quad \dots(1.1)$$

Where $\left(\frac{\lambda_c}{n}\right)$ the wavelength within the material, and Q and v is are the quality factor and mode volume of cavity, respectively. Cavities with smaller mode volume¹ will have larger enhancement in the spontaneous emission.

Fabricating cavities of higher Q is of great interest to understand enhanced light matter interactions¹⁷. In this context, spherical microcavities^{17,18} have gained tremendous attention due to their high Q factor of 10^{11} , compared to values around 10^5 for best Fabry-Perot

¹Cavities with smaller physical dimensions don't imply smaller mode volumes.

resonator. The resonance modes of spherical microcavities are termed as whispering gallery modes¹⁸. The name whispering gallery modes comes from John William Strutt (Lord Rayleigh), who studied the characteristics of the so-called Whispering Gallery of acoustic waves at the dome of St Paul's Cathedral in London, at about 30m above the floor¹⁸. It had got this name because a small whisper against its wall at any point is audible to a listener with an ear held to the wall at any other point around the gallery. Optical whispering gallery modes are observed in varieties of structures including spherical cavities, but here we restrict our discussion to spherical cavities which has more relevance with this thesis.

Spherical microcavities made of dielectric material, where optical rays are totally internally reflected and focused by the surface itself sustain whispering-gallery modes (WGMs), which can be interpreted as electromagnetic waves that circulate and are strongly confined within the sphere as shown in [figure 1.1\(a\)](#). Due to minimal reflection losses and potentially very low material absorption, these modes can reach exceptionally high quality factors^{12,18}.

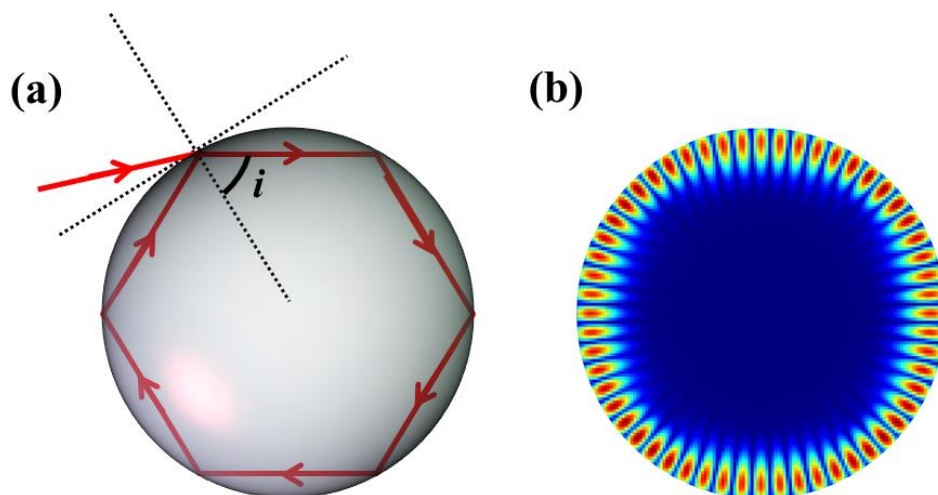


Figure 1.1: Whispering Gallery Modes. (a) Schematic ray picture of light confinement in a microsphere by total internal reflection on the surface. (b) Finite difference time domain (FDTD) simulation for 5 micron SiO_2 sphere having refractive index of 1.46; periphery of sphere shows discrete maximum intensities along the circumference.

As mentioned above spherical microcavities sustain WGMs, these modes have equatorial, radial, as well as polar field dependencies. WGMs can be viewed as high angular momentum electromagnetic modes in which light propagates by repeated total internal reflection with proper phase condition after circling along the sphere surface. As shown in [figure 1.1\(a\)](#), a ray of light propagating inside, hitting the surface with angle of incidence i , which is greater than the critical angle ($\arcsin(1/N)$; $N = RI$) the total internal reflection occurs. This

simple geometric picture leads to the concept of resonance. For large microsphere ($a \gg \lambda$; $a = \text{radius of sphere}$), the trapped ray propagates close to the surface, and transverse a distance $= 2\pi a$ in a round trip. If one round trip exactly equals l wavelengths in the medium ($l = \text{integer}$), then one expects a standing wave to occur. This condition translates into

$$2\pi a \approx (\lambda/N) \quad \dots(1.2)$$

since (λ/N) is the wavelength in the medium. In terms of the size parameter the resonance condition is

$$x = 2\pi a/\lambda \approx l/N \quad \dots(1.3)$$

The number of wavelengths l in the circumference can be identified as the angular momentum in the usual sense. Ray optics or the eikonal approximation may reveal many of the features of the WGM's¹⁸. However Lorentz – Mie¹⁹ theory provides strict analytical solution to the scattering by the spherical microcavities. We utilized this theory to calculate parameter of scattered radiation, see [Appendix](#). Numerical calculations can be done to visualize the electric fields concentrated along a circumference of a sphere (see [figure 1.1\(b\)](#)). Different resonance modes of spheres can be distinguished by the number of intensity maxima's along radial and azimuthal direction, [figure 1.1\(b\)](#) is electric field map for TE_{44,1} more details are discussed in [Appendix](#) and [Chapter 3](#).

1.2. Optical Waveguides

Transporting light from one point to another effectively without divergence has importance in the context of optical communication. Optical fiber does this job of transmitting light over thousands of kilometres without much loss (less than 1dB)²⁰. Commercial optical fibers have diameters around tens of microns. Further decreasing the diameter size of an optical fiber reduces the number of modes coupling to the fiber⁴ (classical diffraction limit). This is the major hindrance in miniaturizing optical fibers down to subwavelength scales and further integration with nano-phonic devices. On the other hand today's electronic chips are manufactured using 30 nm fabrication of copper or silicon for signal processing²¹. But the processing speed is limited by the speed of electrons.

Harvesting light for on-chip signal processing at nanometre scale will allow for sufficient miniaturization of chips and provide high processing speeds, which are required to revolutionize the current available technology. This has motivated researchers to design new

ways to transport light through channels of sizes much smaller than the wavelength of light²²⁻²⁴. Surface plasmon polaritons (SPPs) or exciton polaritons (EPs), which are coupled oscillations of electrons on metal or electron-hole pairs in semiconductors coupled with electromagnetic waves, have been harvested to propagate light at nanoscales. Herein I will introduce to these two concepts of SPPs and EPs and their relevance in nano-optics in the context of this thesis.

1.2.1. Surface Plasmon Polaritons (SPPs)

Collective oscillations of electrons coupled with light on metallic nanostructures are termed as surface plasmons (SPs)²⁵. SPs can be of two types; first, localized surface plasmons (LSPs)²⁶ where SPs are confined to small interaction volumes and facilitate large optical densities. Second, surface plasmon polaritons (SPPs)²⁶ where SPs propagate along metal-dielectric interface. LSPs are utilized for optical sensing²⁷ whereas SPPs are employed for waveguiding^{28,29}. Here I will concentrate SPPs but note that LSPs are also harvested for waveguiding through chains of metal nanoparticles.

Among various plasmonic structures are proposed and demonstrated for optical waveguiding property, chemically synthesised 1-dimensional silver³⁰ or gold³¹ metallic nanowires gained significant interest. Because chemically synthesised nanowires are single crystalline and transport light with minimal propagation loss³². Apart from waveguiding property, nanowires have been used to realize polarization based logic gates³³, Fabry-Perot resonators³⁴, plasmonic routers³⁵ and beam splitters³⁶, surface enhanced Raman scattering³⁷⁻⁴⁰, enhanced fluorescence⁴¹ etc.

How does 1-dimensional metallic nanowire can propagate light below diffraction limit whereas dielectric waveguides doesn't? Consider a relation derived from classical optics²⁶, in order to propagate the radiation in one direction (say z axis) and with propagation constant β ,

$$\beta^2 + k_x^2 + k_y^2 = \epsilon_{core} \frac{\omega^2}{c^2} \quad \dots(1.4)$$

where k_x and k_y are the transverse components of the wave vector, ϵ_{core} is the relative permittivity of medium and ω is the frequency of radiation. For dielectric core $\epsilon_{core} > 0$ and k_x, k_y are real. This implies that

$$k_x, k_y, \beta \leq \sqrt{\epsilon_{core}} \left(\frac{\omega}{c} \right) = 2\pi n_{core} / \lambda_0 \quad \dots(1.5)$$

with this we can conclude that mode size of optical wave is limited by the effective wavelength in the core medium. But if the core is made of metallic then $\epsilon_{core} < 0$ to full fill the condition k_x, k_y must be imaginary and the inequality doesn't hold for this system, further mode sizes can be below diffraction limits.

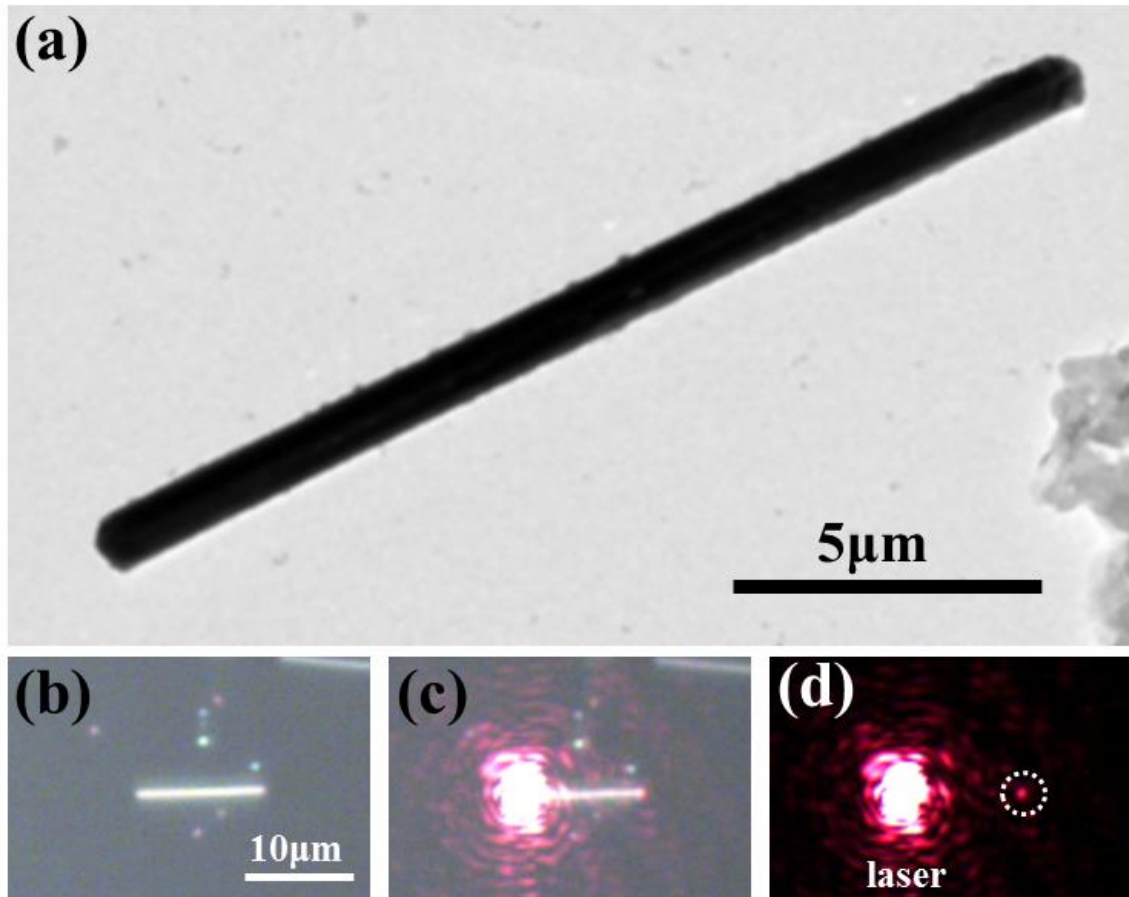


Figure 1.2: Propagation loss in Silver nanowire. (a) TEM image of single isolated silver nanowire of length 15 μm and diameter of 112 nm. (b) optical microscope image isolated silver nanowire; (c) optical image of focused laser beam 632.8 nm wavelength illuminating on the end of the nanowire, captured in the presence of white light illumination. (d) Optical image of (c) captured in the absence of white light, dotted white circle indicates position of out coming light from the other end of nanowire.

Another concept which is important to be addressed in the context of nanowires as waveguides is the losses associated with the propagation. Consider a silver nanowire (AgNW) of fixed length and diameter, see [figure 1.2](#). On excitation of SPPs on silver nanowire through focused laser light (though an objective lens 100x, NA=1) of fixed wavelength at the end of nanowire, plasmons propagate long the length of nanowire and decoupled back into free photons on the other end, see [figure 1.2\(d\)](#). Knowing the input

intensity at one end of the nanowire and measuring the intensity at the distal end, losses associated with the propagation can be estimated. It is calculated that propagation loss in these system is 0.8 dB/ μm . Detailed analytical way³² to measure propagation loss will be discussed in [chapter 2.2](#). Note propagation losses in these system is not compared with optical fibers. Plasmonic waveguides are studied in the context of finding application in nano-phonic circuits rather than long range communications.

SPs of Silver nanowires (AgNW) have become a promising technique to beat the diffraction limit and guide the light up to 20 μm in length^{11,29,42}. But on one side Ag is prone to oxidation with time and SPs is not an ultimate solution to the problem, because of the losses associated with the resistive heating⁴³⁻⁴⁷ within the metal limits the maximum propagation length. With this it becomes increasingly important to use low-loss optical waveguides fabricated from various dielectric, inorganic or organic material. This brings us to the new functional optical materials called photonic nanowire.

1.2.2. Organic waveguides (Exciton polaritons)

Over the past decade, nanostructures based on organic molecules have emerged as potential candidates for optical elements in modern photonic devices⁴⁸, mainly because of their diverse tuneable properties²⁴, high photoluminescence efficiency⁴⁹, better waveguiding abilities^{50,51}, cost-efficient synthesis, unique non-linear optical properties⁵² and good processability⁵³. The optical properties of organic nanostructures arise from the highly ordered π – stacked molecules.

Of the organic nanostructures, one dimensional waveguide structures have drawn great deal of interest due to their variety of optical properties such as polarized emission, lasing⁵⁴, enhanced emission, waveguiding^{50,55,56}. They can be easily adapted for multiplexed nanophotonics application involving nano-optical waveguiding⁵⁷, lasers⁵⁴, light-emitting diodes, transistors⁵⁸ and optoelectronics. These crystalline nanostructures consist of luminescent molecules with low molecular weight and can be synthesized using simple and mild preparation methods. Most of the unique optical properties of these nanostructures are due to their high luminescence efficiency. One of the most attractive features of these organic molecules-based structures is their tuneable optical properties, which have potential applications in building solid state miniature lasers.

Waveguiding property in quasi 1-dimensional organic nanostructures is via harvesting exciton polaritons (EPs). EPs are the coupled oscillations of electron-hole pair (exciton) with electromagnetic waves⁵⁵. Organic nanowires show remarkable propagation properties because of strong coupling⁵⁹ of excitons with photons leading to low group velocity and large refractive index of medium⁶⁰. Stability of EPs at the excitation point is crucial for propagation of radiation over microscopic distances. The stability of EPs is governed by two factors, exciton binding energy (E_{ex}) and longitudinal – transverse exciton splitting energy ($\Delta E_{L-T} = E_L - E_T$). Propagation of EPs in the medium is possible when $\Delta E_{L-T} \& E_{ex} > kT$; where kT is the thermal energy.

In organic materials Frankel exciton⁶¹ is created on excitation and these excitons are localized on molecules. The typical binding energies associated with these excitons range from 0.1 eV to 1 eV. This means these excitons are stable at room temperature ($kT = 30\text{meV}$) and propagate through the medium on coupling with electromagnetic radiation.

Having provided sufficient background on optical cavities and waveguides I will further present our study on ‘emission characteristics of organic meso/nanowires coupled with plasmonic and dielectric substrates’. The thesis work is diving into four major chapters. [Chapter 1](#): is the introduction to optical cavities and waveguides, which we have currently discussed. [Chapter 2](#): Organic meso/nanowire, here I will present some interesting properties of organic mesowires such as active & passive waveguiding, wavelength dependent propagation and optical antenna effect. [Chapter 3](#): Microsphere coupled organic waveguide, here I will discuss on coupling optical cavities with waveguides, how optical properties and cavity modes are altered will be addressed. [Chapter 4](#): Vertical Nanowires coupled with plasmons, here I will discuss on coupling excitons with plasmons and the polarization states of emitted light.

Chapter 2

Growth and Wavelength Dependent Optical Waveguiding Properties of Organic Mesowire

One of the primary goals of nanophotonics is to design and develop nano-optical elements that can be harnessed to propagate and localize light at subwavelength scales. In order to achieve this goal optical waveguides^{62,63} at the micro/nanoscale have been synthesized, grown or fabricated with different materials and classified under inorganic semiconductor waveguides⁶⁴, polymer dielectric waveguides⁶⁵, plasmonic waveguides²⁸ and organic waveguides⁶⁶. There are two types of waveguiding properties are associated these waveguides namely active⁶⁷ and passive⁵³ waveguiding. In passive waveguiding, waveguides propagates the input light to the output, without change in the frequency of the input light. Whereas in active waveguiding, single input frequency light leads to molecular/atomic excitations and output light contains multiple frequencies along with the input frequency. Both active waveguides and passive waveguides have their own technological advantages.

Among various kinds of waveguides, organic waveguides made of small molecules (Molecular weight \approx 250) have gained tremendous interest^{50,56}, mainly because of low propagation loss associated with the waveguides and flexibility in tuning the optical properties of building blocks (molecules). Organic waveguides can serve as both passive and active waveguides, depending on the frequency of excitation with respect to absorption window of molecules used for building the waveguides. Organic waveguides are different from those “passive optical waveguides” like silica optical fibres, organic waveguides contain different kinds of active light materials that can be excited by the external light source, which guide the emitting light instead of the incident light. Organic waveguides are

1-dimensional crystalline material in which highly ordered stacking of pi-conjugated molecules⁶⁸ offer better stabilities⁶⁹ and charge transport properties^{70,71}, which result in better photonic performances of the final devices. Some unique applications, like tuneable colour displays^{70,72-74}, field - effect transistors⁵⁸, chemical sensors⁷⁵, and lasers^{24,54,76} have been achieved.

When we discuss about waveguiding property there are three important features which need to be commented, they are 1) Propagation losses, 2) wavelength dependency (bandwidth) and 3) directionality of out coming light. These are the three key things that will be discussed in this chapter. Chapter starts with the growth of organic waveguides grown from small molecule named 1,5-diaminoanthraquinone (DAAQ), which is extensively used in dye industry^{77,78} and goes on with discussion on these key points.

2.1. Growth of Organic Waveguides

The 1,5-diaminoanthraquinone (DAAQ) waveguides were prepared by vapour deposition method^{77,78}. In a typical preparation, 10 mg DAAQ powder was dissolved with 40 ml of ethanol in a 100 ml 2-necked round bottom (RB) flask. The RB flask was then placed in silicon oil bath and the temperature was increased up to 60 °C to evaporate the ethanol. A gradual evaporation of ethanol left a solid uniform thin layer of DAAQ film on the inner wall of RB flask, as shown in [figure 2.1\(a\)](#).

A glass cover slip (or ITO coated glass slide) was cleaned with detergent and rinsed in deionised water. Then it was washed with acetone followed by drying. This glass cover-slip was used for sub-sequential growth of DAAQ molecular waveguides. Then a glass substrate was perpendicularly suspended into RB flask. The oil bath was subsequently heated up to 170 °C, and monitored by a sensor inserted into the RB flask from other neck. DAAQ molecules vaporized from the inner wall of RB flask and got condensed on the glass substrate which is at lower temperature. Growth of DAAQ waveguides involves two important steps namely, nucleation and anisotropic growth. During nucleation process countable numbers of DAAQ molecules condense locally forming a cluster called nuclei, $\pi - \pi$ stacking interaction among the molecules and thermal diffusion of molecules on substrate play an important role in determining the orientation of nuclei. These nuclei act preferred condensation sites for subsequent condensation of DAAQ molecules. The anisotropic structure of DAAQ molecules assists the growth along 1-dimension, whereas other two dimensions are confined to 600 –

700 nm. After 15 min of deposition, the glass substrate was removed from the flask and further visualized using an optical microscope. Optical images were captured through different microscopes working in three different configuration namely back scattering mode, transmission mode and dark-field configuration.

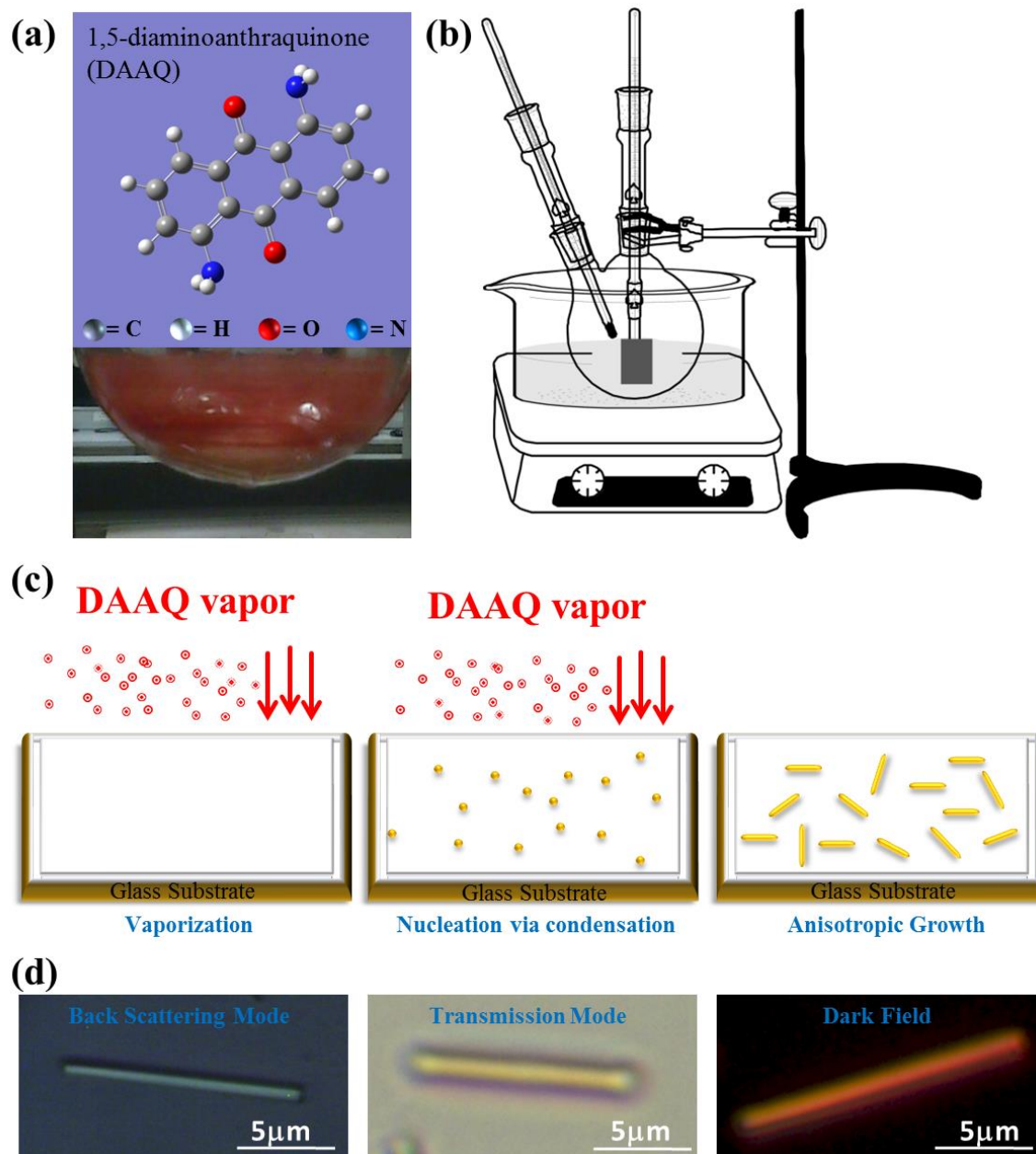


Figure 2.1: Growth of Organic Mesowire. (a) (Top) Chemical structure of 1,5-Diaminoanthraquinone (DAAQ) molecule. (Bottom) Optical image of round bottom (RB) flask uniformly coated with DAAQ molecules. (b) Setup used for the growth of organic mesowires. (c) Schematic illustration for the growth process of organic mesowire via physical vapor deposition (PVD) technique. (d) Optical images of isolated organic mesowire captured using 100x (NA = 1) in three different configuration namely, back scattering mode, transmission mode and dark field.

Length and diameter of these mesowires can be controlled⁷⁸ by varying the deposition time and evaporation temperature respectively. In most of the experiments deposition time was 15 min and evaporation temperature was 170 °C, which resulted in lengths of 20±5 μm and diameter of 700±100 nm.

2.2. Light Propagation (Exciton Polaritons)

In order to test the light propagation capabilities, we microscopically identified isolated organic mesowire and focussed 633 nm (He-Ne laser) light through a high NA objective lens (100×, 0.9 NA) at one end of the wire and captured the optical images. [Figures 2.2\(b\)](#) and [2.2\(c\)](#) are CCD images of end illuminated organic wire of length 19μm in the presence and absence of a background white-light illumination, respectively. The arrow in [figure 2.2\(c\)](#) represents the incident electric field polarization. We observed bright spots at the other end of the mesowire. In [figure 2.2\(d\)](#), we show the three dimensional representation of the optical image displayed in [figure 2.2\(c\)](#). Two different peaks were observed that represented: an intense peak of input light and an emission peak at the other end of the mesowire. Light incident at one end of the mesowire results in formation of excitons (electron hole pairs), the collective oscillations of the excitons coupled with electromagnetic wave known as exciton polaritons (EPs) propagate through the mesowire. At the distal end of the mesowire EPs convert back into free photons due to boundary discontinuity, which is observed as a second peak in the 3-dimensional representation of [figure 2\(d\)](#).

We estimated the propagation loss^{32,78} (α) of the organic mesowire. The propagation loss α is inversely proportional to propagation length L_o as

$$\alpha = \frac{-10 \times \log(\frac{1}{e})}{L_o} \approx \frac{4.343}{L_o} \quad \dots(2.1)$$

Where L_o is propagation length over which the intensity decreases to 1/e the initial values. The propagation length of organic mesowire can be estimated from the light intensity from the distal end of the mesowire, which exponentially decreases as

$$I(x) = I_o \times e^{-x/L_o} \quad \dots(2.2)$$

where I_o is the initial intensity and x is the local position along the length. By measuring the output intensity at the distal end of the wire from 3-dimensional representation, (figure 2(d)) propagation length L_o was measured and found to be 959.5 μm at 632.8 nm. Corresponding

propagation loss was found to be $0.0045\text{dB}/\mu\text{m}$. Measured propagation loss in organic mesowire is very small compared to propagation losses associated with plasmonic nanowires (see, [chapter 1.2.1](#)), where loss arise due to heating effects and propagation losses^{43,44} can be as high as $0.8\text{dB}/\mu\text{m}$ at 633 nm .

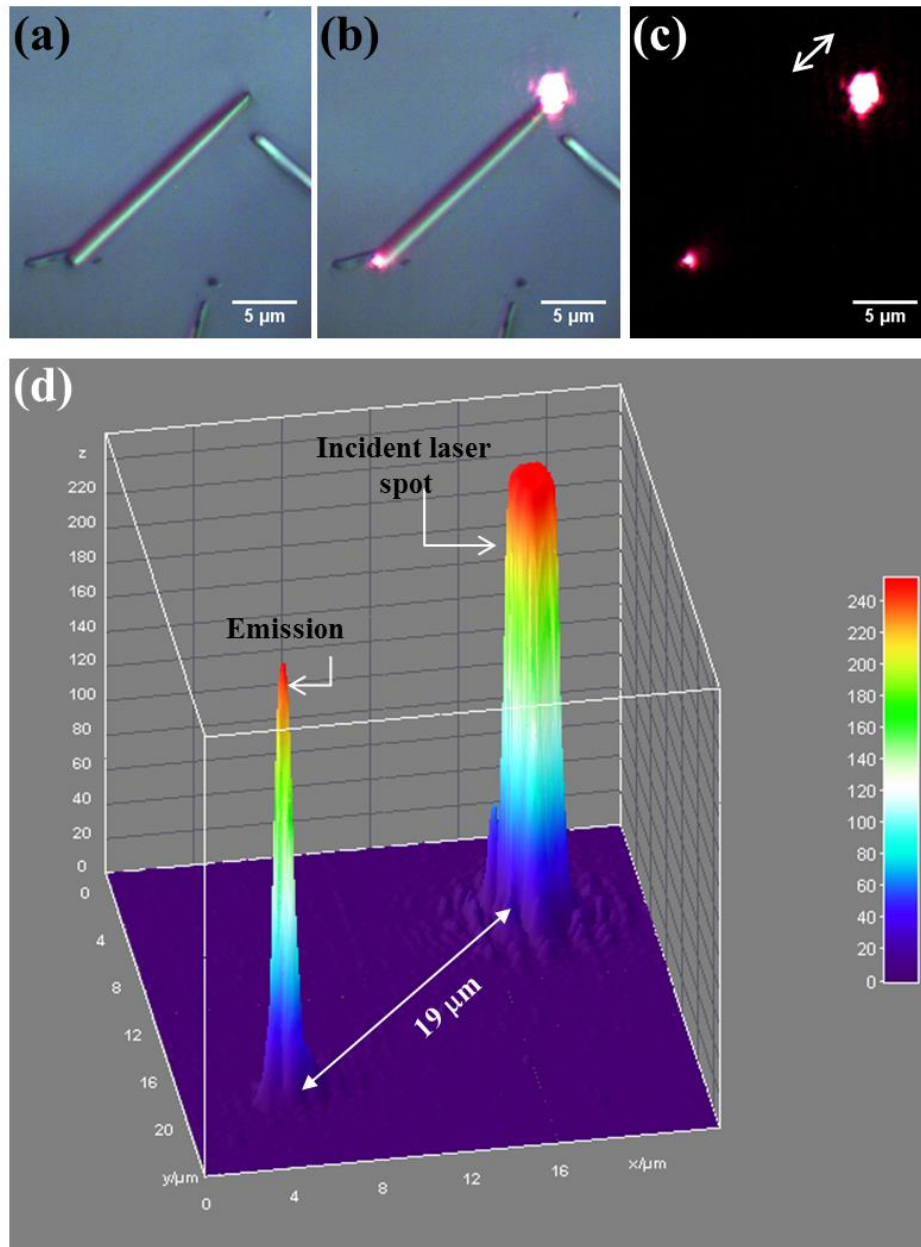


Figure 2.2: Light Propagation via exciton polaritons. (a) Optical microscope image of isolated organic mesowire. (b) Optical image of focused laser beam 632.8 nm wavelength illuminating on the end of organic mesowire captured in the presence of white light illumination. (c) Optical image of (b) captured in the absence of white light. (d) 3-D projection of optical image in (c) indicating the input light and the emitted light.

2.3. Wavelength Dependent Propagation

What is the wavelength dependent response of these organic mesowires? In order to address this question, white light extension (absorption + scattering) spectrum of organic mesowires grown on transparent glass substrate was collected and compared it with the wavelength response of DAAQ molecules dissolved in ethanol, shown in figure 2.3(a). DAAQ molecules in solution form exhibit two resolved absorption bands at 295 and 490 nm. The peak at 295 nm is attributed to $\pi \rightarrow \pi^*$ ($2^1B_u \leftarrow X^1A_g$) transition, while peak at 490 nm is also attributed to intermolecular charge transfer⁷⁷ between adjacent NH_2 and $C=O$ groups. In contrast with discrete energy levels in DAAQ molecules, formation of different energy bands is observed in mesowires. Weak inter-molecular interactions such as hydrogen bonds, π - π stacking, van der Waals and charge transfer contacts are main reason for energy level coupling of adjacent molecules. Due to molecular aggregation red shift in the absorption bands was observed.

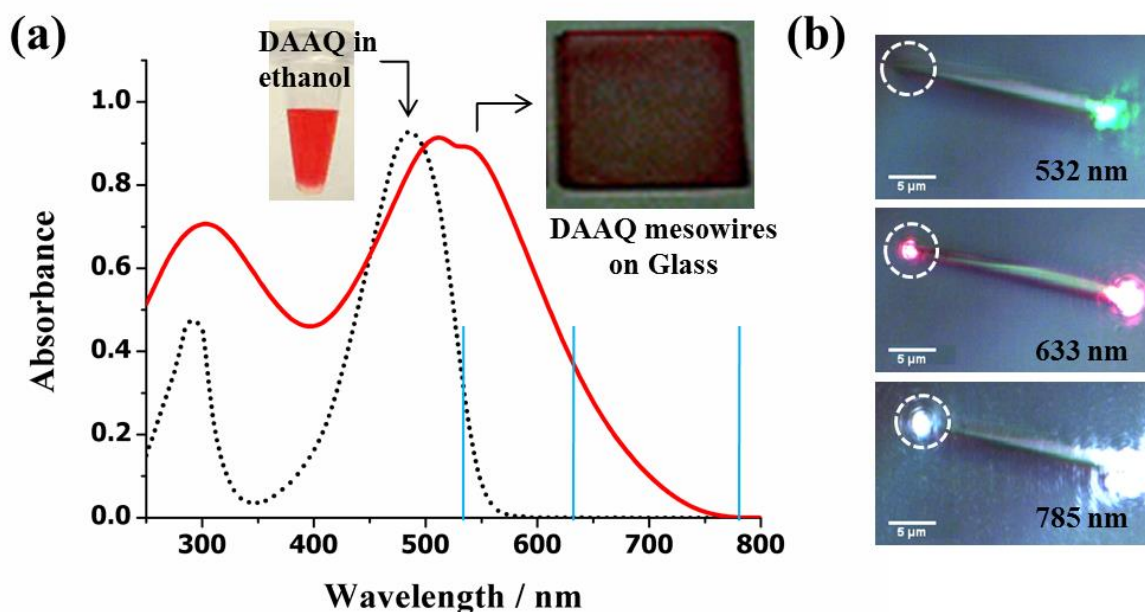


Figure 2.3: Wavelength Dependent Light Propagation Properties. (a) (black dotted line) Absorption spectrum of DAAQ molecule in ethanol solution. (Solid red line) Absorption spectrum of organic mesowire grown on the glass substrate. Inset shows the images of respective samples. Solid blue lines are the wavelength points at which propagation properties are measured. (b) Optical image of focused laser beam of different wavelength (top) 532 nm, (middle) 633 nm and (bottom) 785 nm, illuminating on the end of organic mesowire captured in the presence of white light illumination.

Having difference in extension cross-section for different wavelength, does the propagation property of mesowire depend on the input wavelength? This question is addressed by doing propagation studies at multiple wavelengths (532, 633 and 785 nm). These three different wavelengths were marked with blue vertical lines on the extension spectrum of mesowire, [figure 2.3\(a\)](#). Experiments were done on custom built Raman microscope (LabRam HR, Horiba JobinYvon, France). Optically isolated mesowire was identified and laser of different wavelength (one at a time) was focused through a high NA (=1) objective lens. CCD images of laser illuminated mesowire were captured, shown in [figure 2.3\(b\)](#).

For 633 and 785 nm laser incident, propagation along the nanowire was observed and emission from the other end was detected in CCD images, [figure 2.3\(b\)](#). Whereas for 532 nm excitation, emission from the opposite end of mesowire was not observed, [figure 2.3\(b\)](#) (top). Waveguiding depends upon the solid state absorption window of molecular building blocks. Hence to achieve light propagation excitation with longer wavelength beyond the molecular absorption window is crucial.

2.4. Directional Emission (Antenna effect)

An antenna works as a converter between electromagnetic radiation and electrical signals. The concept of antenna is well established in the radiofrequency (RF) and microwave (MW) regime due to widespread use in the field of telecommunication and astronomy⁷⁹. But the optical counterpart of antenna has not made its way into technological applications. The main hindrance for this was to fabricate well defined nanostructures of the antenna. But recent developments in the field of nanosciences have made it way to articulate nanostructures. Like classical antenna the primary objective of optical antenna is to optimize energy transfer between localized source and free radiation field. Now unidirectional RF antenna like Yagi-Uda⁸⁰, are designed for optimized reception of signal fed from the specific direction. In same way it can also emit electromagnetic radiation in directed manner once fed by properly positioned electrical source. On a similar note there is need for unidirectional optical antennae, which can direct a localized signal from a subwavelength volume towards a specific direction. To fulfil this requirement antenna elements have to be placed in such a manner that interferences happen to be constructive in one direction and destructive in the opposite direction⁸¹. These directional antennae are very important for developing different optical sensors and molecular spectroscopy techniques⁸².

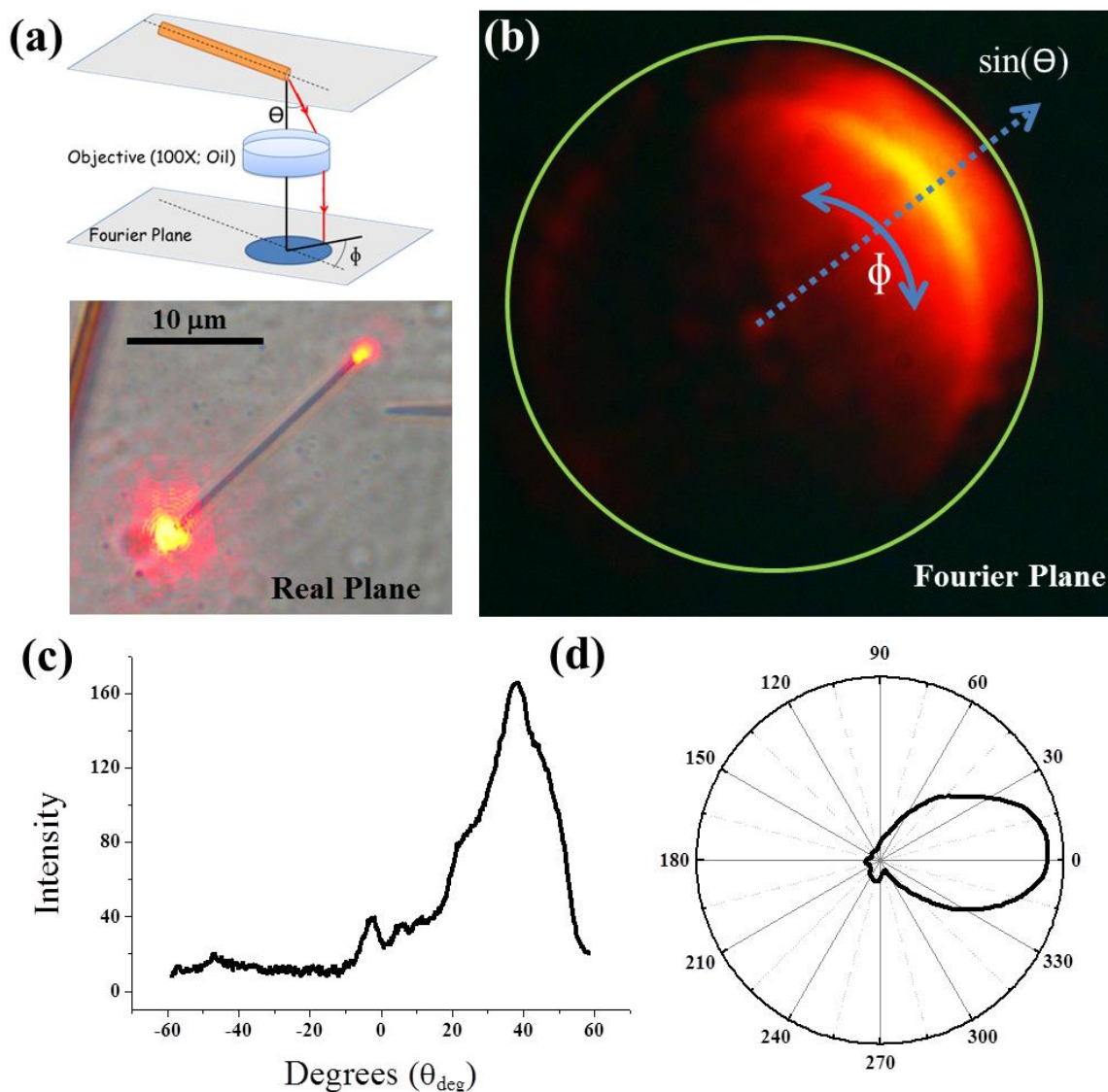


Figure 2.4: Optical Antenna – Directional emission. (a) (Top) Illustration of the detection scheme and the coordinate system used. (Bottom) Real plane optical image of focused laser beam 632.8 nm wavelength illuminating on one end of the organic mesowire. (b) Corresponding Fourier plane image of emitted light, captured by spatially isolating the emitted light and in the absence of white light illumination. (c) Radial (θ) intensity variation calculated from Fourier plane image. (d) Azimuthal intensity variation at (θ_{max}) plotted in a polar coordinates.

Plasmonic materials can squeeze light into subwavelength dimensions due to interactions between incident light and free oscillating conduction band electrons, known as plasmons. Now, it is well known that novel metal structures such as nano particle dimer⁸³, bowtie antenna⁸⁴ and subwavelength apertures⁸⁵ etc. can focus light to nanometric volumes. But they don't provide any kind of unidirectional emission because significant amount of phase

retardation is required for the emission to be unidirectional. Recent developments in the field suggest Rf inspired optical Yagi-Uda⁸⁶ antenna and metal nanowire⁸⁷ can act as unidirectional antenna, providing very high degree of unidirectionality up-to 15dB. Despite of being highly unidirectional, one has to deal with large amount of losses happening due to Joule heating in these plasmonic antennas. Organic excitonic mesowires can be a good alternative to overcome this problem. We have already demonstrated that these mesowires can propagate light from one place to other by means of propagating exciton polaritons. When one of the ends of these wires is excited with proper source light propagates and emits at the distal end. Herein we will show that emitted light is highly unidirectional.

To characterize the directionality of emission from the distal end we have used a method called Fourier space microscopy. In this technique light from the sample is collected using a high numerical aperture (N.A.) objective lens and backfocal plane of the objective is examined. Direct monitoring of back focal plane facilitates angular characterization of distribution of the emitted light intensity in terms of spherical coordinates θ and ϕ as defined in [figure 2.4\(a\)](#). [Figure 2.4\(a\)](#) shows a schematic of the experimental setup. We used a 633 nm He-Ne laser as excitation source. The laser was focused on to one of the ends of the mesowire by a 100 \times . 1.3 N.A. objective lens. The emitted light was collected using the same objective. Then the collected light was directed towards a 4f correlator. The first lens of the correlator creates an intermediate real image plane to provide the capability of spatial filtering. Only the light emitted from the distal end was filtered out and incident laser was blocked using a circular aperture at this plane. Then we used a tube lens mounted on a flip mount to capture real image using an imaging CCD. Once this lens is flipped out of the path, the ccd is focused at the back focal plane of the objective and Fourier plane image is captured.

[Figure 2.4\(b\)](#) is a real image of the light propagation through an excitonic wire. The light emitting from the distal end (portion of image marked by the dotted circle) was put into the ccd. [Figure 2.4\(c\)](#) is the captured Fourier plane image of the part of the mesowire contributing to the far field radiation. The radial coordinate in the Fourier image scales as the numerical aperture ($N.A. = n \sin \theta$) where $n = 1.518$, while the tangential coordinate corresponds to the angle ϕ ($0 < \phi < 2\pi$). The dotted circle in figure 2.4(c) represents $N.A. = 1.3$, numerical aperture of the used objective. Observed red circular arc is the highly directional emission from the nanowire end. We estimated the intensity variation as a

function θ and ϕ . From [figure 2.4\(c\)](#), intensity variation along radial direction is measured and plotted in θ_{deg} coordinate, (see [figure 2.4\(d\)](#)) it can be read that intensity peaks around $\theta_{\text{max}} = 38.6^\circ$ and has a spread over FWHM = 8.2° . Azimuthal variation (ϕ) can be found in [figure 2.4\(e\)](#), where it is evident that the maximum emission occurs in the direction of wire orientation. Very low amount of light could be observed in the backward direction ($\phi = \phi_{\text{max}} + 2\pi$), which clearly say that the organic wires are acting as a unidirectional optical antenna. The unidirectionality is measured in terms of front to back scattered light intensity ratio, which turns out to be dB.

To conclude organic mesowires have very unique characteristics which are not available in other systems. Ease of preparation via vapour deposition technique provides surfactant free, non-capping agent and solvent free mesowire (zero contamination). Low propagation loss and broad-band light propagation capability of these mesowires make them better candidates for nano-photonics circuitry. Further directional emission property associated with the light coming out from these mesowires make them potential candidates for building micro/nano antenna, which were missing in optical regime.

Chapter 3

Microsphere Coupled Organic Mesowire: Remote Detection of Whispering Gallery Modes

This chapter constitutes the following publication:

- Microsphere-coupled organic waveguide: preparation, remote excitation of whispering gallery modes and waveguiding property

Rohit Chikkaraddy, Arindam Dasgupta, S. Dutta Gupta, G. V. Pavan Kumar

Applied Physics Letters, 103, 031112 (2013)

How to efficiently transport light through one-dimensional micro and nanostructures? How can such structures be used for multiple optical functions? These are some of the important questions in micro and nanophotonics, and a tremendous amount of research has been directed to answer such questions^{88,89}. In recent times, optical micro and nanostructures made of organic molecules have captured attention because they are versatile and flexible in nature⁹⁰⁻⁹³. In the context of “green photonics”⁹⁴, organic nanostructure may play an important role in facilitating some building blocks of optical devices including waveguiding property. Molecules that facilitate excitons can be harnessed to prepare one-dimensional waveguides. The transport of light in such molecular structures is assisted by exciton-polaritons, which are essentially coupled modes of electromagnetic waves and excitons^{95,96}. These collective excitations have interesting mode characteristics that can be excited beyond optical diffraction limit⁵⁶, and hence attractive candidates for nanophotonics^{51,97-99}.

High quality optical resonators that facilitate large optical powers in confined volumes over extended periods of time is important for various applications in photonics¹². Dielectric microsphere resonances based on whispering gallery modes (WGMs) are one such high quality resonator configuration that has been extensively studied¹⁰⁰⁻¹⁰⁴. The WGMs are electromagnetic waves that circulate near the surface of the microsphere leading to extremely high quality factors. As these modes are characterized by low mode volume and large local field enhancement, they have been harnessed for various applications such as biochemical sensors¹⁰⁵⁻¹⁰⁷, microlasers¹⁰⁸, non-linear optics^{109,110}, optical filters¹¹¹, temperature sensors¹¹², test beds for cavity quantum electrodynamics¹¹³, cavity optomechanics¹¹⁴ etc. The WGMs in microspheres can be excited with various optical schemes based on prisms, integrated waveguide, tapered fiber, angled polished-fiber, and so on.

In the context of WGMs, coupling of microspheres to waveguides made of organic molecules is yet to be achieved, and doing so can be useful because they can be harnessed as versatile and flexible micro-/nano-photonics detection platforms. In such a configuration, the WGMs of the microsphere can be utilized for signal processing (active element), and the organic waveguide can be utilized for signal transmission (passive element). Additionally, these active and passive functions can be interchanged between the microsphere and organic waveguiding, leading to interesting prospects in photonics.

Motivated by the above-mentioned potentials, herein we report on our experimental studies performed on microsphere-coupled organic waveguide (MOW) structure. In this letter, we

show (i) how organic waveguides can be directly grown on a microsphere; (ii) how MOW structure can be used to remotely excite and detect WGMs of microsphere; and (iii) what are the alterations in waveguiding property of MOW structure compared with conventional organic waveguide.

3.1. Fabrication of Microsphere coupled Organic Mesowire

First, we discuss the bottom-up fabrication of MOW structures. A glass cover slip (or ITO coated glass slide) was cleaned with detergent and rinsed in deionised water. Then it was washed with acetone followed by drying. Next, a drop of the solution containing microspheres (5.23 μm silicon beads dispersed in water) was gently drop-casted on the cleaned glass slide and dried at room temperature in a dessicator for 3–4 h. This microsphere drop-casted glass cover-slip was used for sub-sequential growth of 1,5-diaminoanthraquinone (DAAQ) molecular waveguides. The DAAQ waveguides were prepared by vapour deposition method^{77,78}. In a typical preparation, 10 mg DAAQ powder was dissolved with 60 ml of ethanol in a 100 ml 2-necked round bottom (RB) flask. The RB flask was then placed in silicon oil bath and the temperature was increased up to 60 °C to evaporate the ethanol. A gradual evaporation of ethanol left a solid uniform thin layer of DAAQ film on the inner wall of RB flask. Then a glass substrate was perpendicularly suspended into RB flask. The oil bath was subsequently heated up to 170 °C, and monitored by a sensor inserted into the RB flask from other neck. DAAQ molecules vaporized from the inner wall of RB flask and nucleated selectively on the contact area between the microsphere and the substrate, which acts as a preferred condensation sites for DAAQ vapour (see Figure 3.1 for the schematic of the preparation). After 5 min of deposition, the glass substrate was removed from the flask and further visualized using an optical microscope. Figures 3.1(b), (c) show optical images of typical MOW structures obtained by the above-described procedure. A large fraction of the individual microspheres spread on the glass substrate had a single organic waveguide attached to it. Along with the MOW structures, we also observed isolated microspheres that were coated with DAAQ molecules. We used such isolated, coated-microspheres as control samples in our optical experiments.

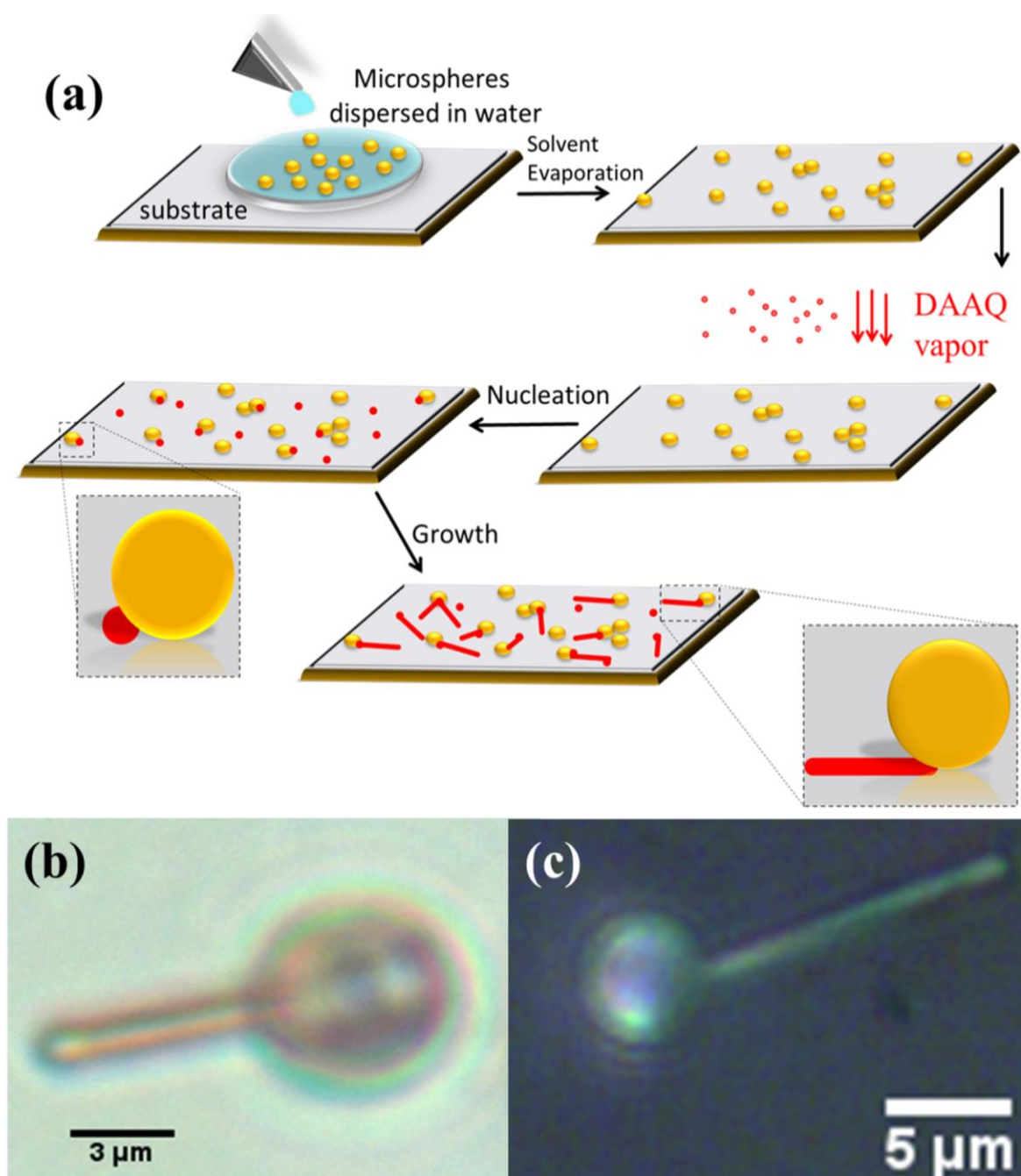


Figure 3.1: Growth of microsphere coupled organic waveguide. (a) Schematic of the preparation of microsphere-coupled organic waveguides (MOWs); (b) and (c) are optical images of two different samples of MOW structures (diameters of wire are ~ 800 nm and ~ 650 nm, respectively).

3.2. Whispering Gallery modes

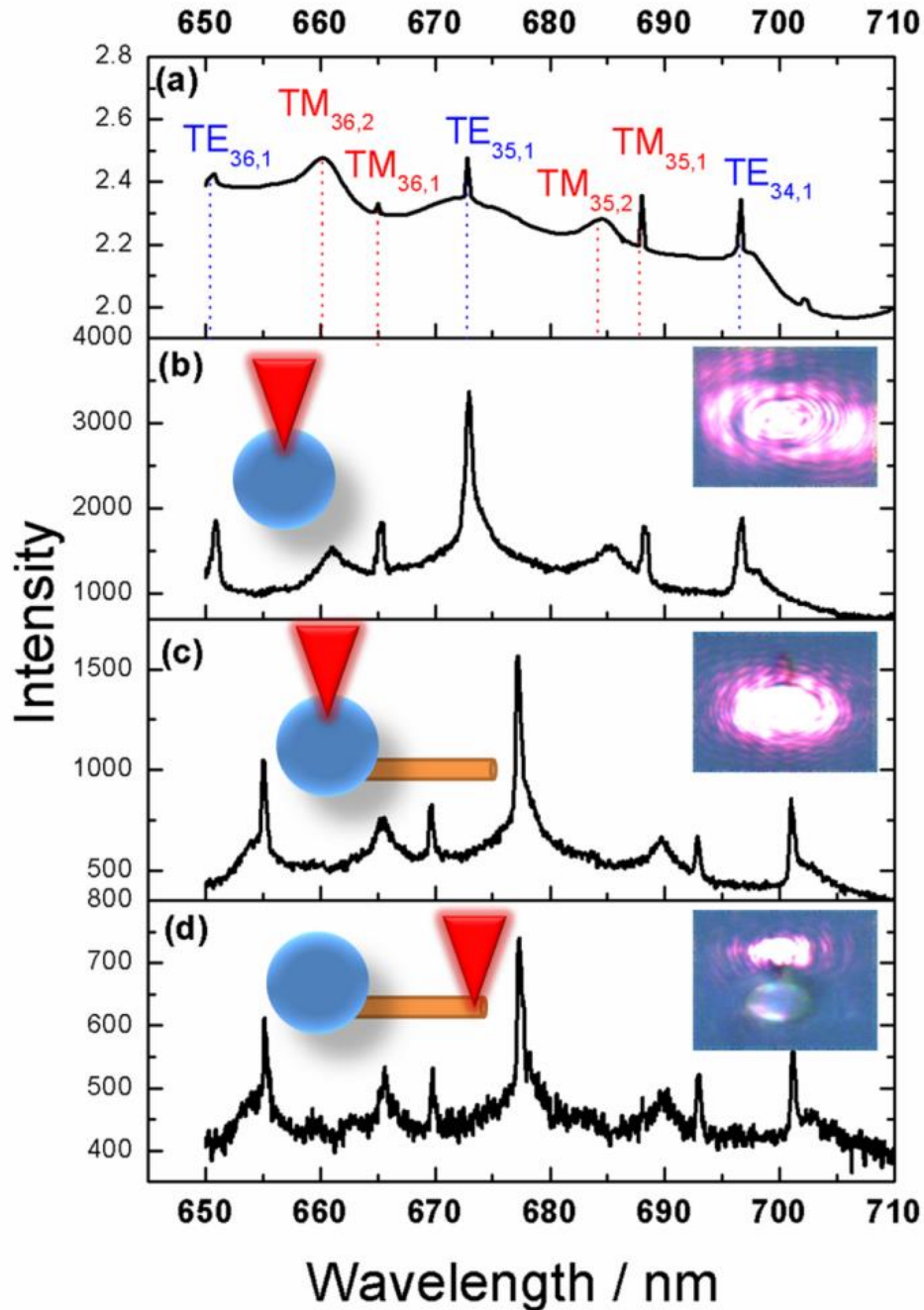


Figure 3.2: Remote excitation and detection of whispering gallery modes (a) Calculated whispering gallery modes by Mie theory for a $5.23 \mu\text{m}$ sphere; experimental results: (b) WGMs from direct illumination of DAAQ coated microspheres; (c) WGMs from illumination of sphere in MOW structure; (d) remotely excited WGMs from illumination of wire in MOW structure. Insets show optical images and schematic of excitation for each case. The laser excitation at 632.81 nm wavelength was through an objective lens ($100\times$, 0.9 NA).

The WGM resonances of a microsphere can be computed using Mie theory, whose details can be found in the supporting information. WGMs of a microsphere are labelled by two polarizations (transverse electric, TE and transverse magnetic, TM) and 3 quantum numbers, namely radial (n), angular (l) and azimuthal quantum numbers (m). The mode number n corresponds to half the number of intensity maximum along the great perimeter of the sphere and mode number l is equal to number of intensity maxima along the radius of sphere. For perfect spheres there is $2n + 1$ fold degeneracy with respect to magnetic quantum number m . Figure 3.2(a) shows the computed WGMs (for $5.23\mu\text{m}$ sphere) from the Mie theory with assigned mode labels. The numbers in subscript indicate quantum numbers n and l .

Next we interrogated the prepared MOW structures using optical microscopy and spectroscopy. First we probed the whispering gallery modes (WGMs) of coated microsphere without an organic waveguide attached to it. For this, we microscopically identified isolated DAAQ-coated microspheres on the above-mentioned glass substrate and focused 632.81nm (He-Ne laser) light through a high NA objective lens ($100\times$, 0.9 NA), and collected the back scattered light through the same channel. The collected light passed through an edge filter to reject the elastic scattered light and a confocal pinhole ($300\mu\text{m}$ diameter) before entering a high resolution optical spectrometer (LabRam HR, Horiba JobinYvon, France). The Stokes scattered light spectra were further utilized to WGM analysis. We compared the computed WGM modes ([figure 3.2\(a\)](#)) to our experimental data obtained with isolated microspheres as displayed in [figure 3.2\(b\)](#). The inset shows the optical image of the illuminated microsphere along with the illumination configuration. We observed a good one-to-one correspondence between the computed and experimental data. The $\text{TE}_{35,1}$ was the strongest mode in the Stokes spectra and the quality factor for this mode was found to be $\sim 0.5 \times 10^3$.

3.3. Microsphere coupled Organic waveguide

Next, we discuss the effect of organic waveguide coupling on the WGM mode of the microsphere. [Figure 3.2\(c\)](#), shows recorded WGMs for MOW structure. In this experiment, the laser beam was focused directly on the microsphere as shown in the inset of [figure 3.2\(c\)](#). The spectral features of the MOW structure with direct illumination showed a systematic red-shift of 5.74nm when compared with the case of isolated sphere without an organic waveguide attachment. This red-shift is due to the conjugation of organic waveguide to the

microsphere which results in the change of effective refractive index. Also, the attachment of organic waveguide breaks the symmetry of the sphere, leading to such changes in the modes.

Can the WGM modes of the conjugated microsphere be remotely excited and detected via organic waveguide? To answer this question, we focused the laser beam on the free end of the organic waveguide whose other end was attached to a microsphere (see optical image in the inset of [figure 3.2\(d\)](#)). [Figure 3.2\(d\)](#), shows the remotely *excited and collected* WGM spectrum, in which laser beam was illuminated at the end of the wire, and the backscattered signal was collected from the same point. It was evident that the remotely excited WGMs ([figure 3.2\(d\)](#)) had exact features as the modes shown in [figure 3.2\(c\)](#), but with a lower intensity. [Figure 3.2\(d\)](#) is the central result of this chapter. It indicates that by exciting distal end of the organic waveguide in the MOW structure, one can remotely excite and detect whispering gallery modes of the sphere. This remote excitation is facilitated by propagating exciton-polaritons in the organic waveguides, where the incident photons are converted into exciton-polaritons, which further propagate along the wire and excite the WG modes. These excited WGMs are further coupled evanescently into the wire that propagates back to the distal end of the mesowires. Although the signal-to-noise ratio of the obtained WGM spectra were good, it is to be noted that there are losses of photons due to excitation coupling, mechanical coupling between waveguide and the microsphere, and due to propagation of exciton-polaritons in the waveguide. Such losses can be minimized by near-field excitation and appropriate fabrication methodologies. Furthermore, it is to be noted that the grown structures due to the attached organic waveguides lack spherical symmetry, and in most cases even the axial symmetry. The WGM cases for axisymmetric deformations have been studied earlier both theoretically¹¹⁵ and experimentally¹¹⁶, reporting on the effects of broken azimuthal symmetry and mode splitting in such geometries. In our case, since the organic waveguide attachment is not along a diameter of sphere, axial symmetry is broken leading to whispering gallery mode mixing phenomena. In what follows, we demonstrate this mode splitting and mixing phenomena with our MOW structures.

3.4. Kramer's Degeneracy

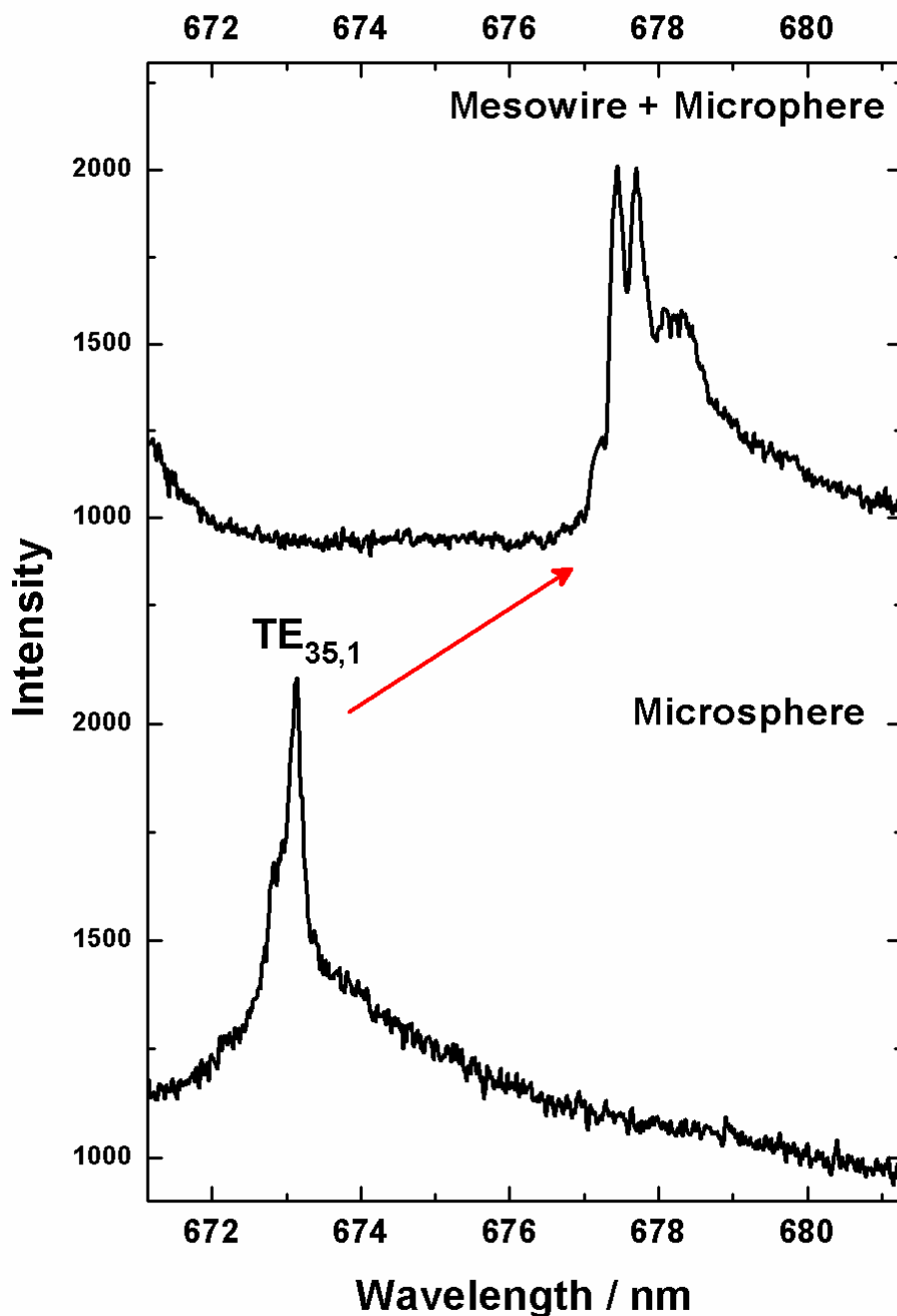


Figure 3.3: Mode splitting and mode mixing phenomenon in MOW (Kramer's degeneracy) Effect of organic waveguide coupling on whispering gallery mode of a ~ 5 micron silica sphere. The lower spectrum is WGM for an isolated sphere. The upper spectrum is WGM for a MOW structure. There is a red-shift and split in the mode due to coupling and azimuthal symmetry breaking in the geometry.

To analyze the WGM mode splitting in MOW structure, we recorded a higher resolution spectrum of the $TE_{35,1}$ mode. [Figure 3.3](#), compares the WGM obtained for isolated sphere with MOW structure. It was interesting to observe that in addition to systematic red-shift in the WGM mode, there was a clear splitting of the modes ([figure 3.3](#), top panel). The observed effects can be explained as follows. In the context of axisymmetric deformation¹¹⁵, it was shown that polarization of the incident wave plays a dominant role in determining the location of the dominant peak (on the left or the right edge) in the split m -resonances. Since, in the current experiment, a tightly focused laser beam was used for WGM excitation, one has comparable contributions from the in-plane polarization (containing the beam central direction and axis of the waveguide) and the perpendicular polarization components, resulting in a mode-splitting phenomenon with almost equal mode intensities. Off-centre organic waveguide also adds to mode-mixing and broadening of these resonances, which was clearly observed in our spectra shown in [figure 3.3](#) (top panel).

3.5. Radiation Pattern

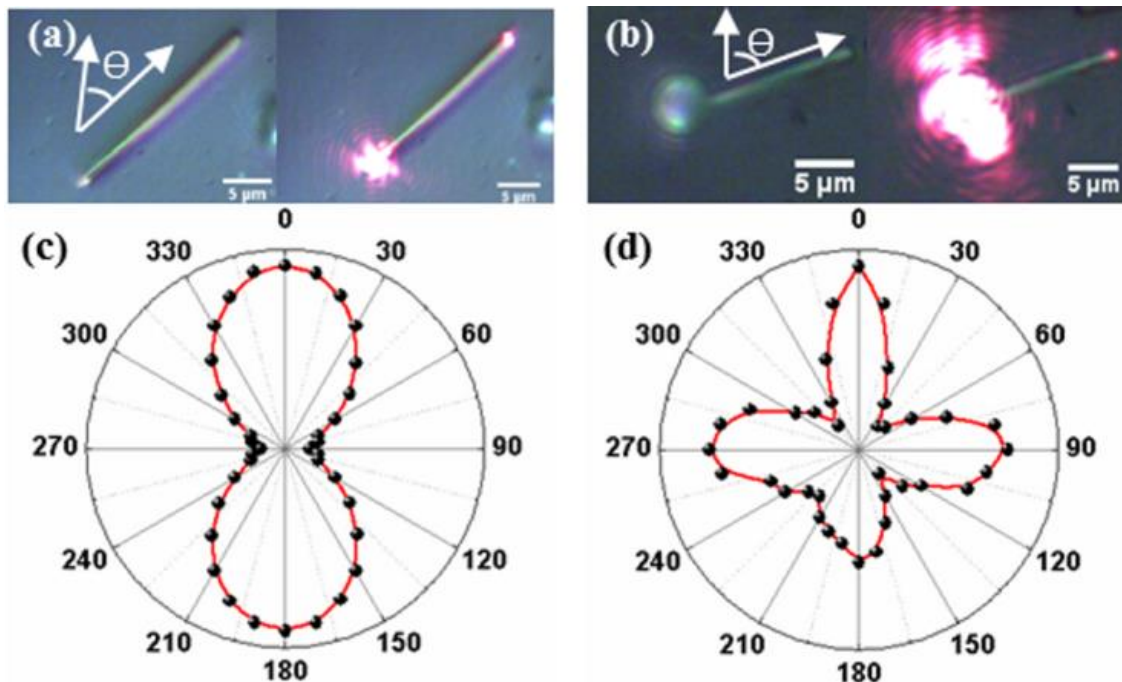


Figure 3.4: Radiation Properties. (a) Optical image showing waveguiding property of an isolated DAAQ waveguide; (b) optical image showing waveguiding property of a microsphere-coupled DAAQ waveguide; (c) polar plot indicating output light intensity as a function input polarization for a DAAQ waveguide; (d) polar plot indicating output light intensity as a function input polarization for a microsphere-coupled DAAQ waveguide.

Until now, we have been discussing the effect of conjugation on the WGMs of the MOW structures. An equally interesting question regarding MOW structures is: how do the waveguiding characteristics of MOW structure differ from a conventional organic waveguide? To answer this question, we compared the input polarization-dependent waveguiding property of an organic waveguide made of DAAQ and compared it to the waveguiding property of the MOW structures. [Figure 3.4\(a\)](#) and b show the optical images of isolated organic waveguide and a MOW structure, respectively. The images have been captured with and without the laser excitation at 632.81nm wavelength. Figure 4c and d are polar plots for organic waveguide and MOW structure, respectively. Polar plot in [figure 3.4\(d\)](#) was plotted by recording the output light intensity at the free end of the wire as a function of polarization of the input light. For the wire case ([figure 3.4\(c\)](#)), the output emission pattern showed a dipolar variation. In contrast to this, the output emission pattern of the MOW structure exhibited quadrupole emission characteristics. The variation of emission pattern from dipole to quadrupole is a consequence of spherical symmetry breaking due to coupling of wire to sphere. Such variation in the emission patterns of a photonic waveguide element would be relevance in nanophotonic circuits where a small-scale change in the geometrical configuration can lead to significant change in the light emission characteristics.

3.6. Conclusion

To conclude, we have shown how a microsphere coupled to an organic cylindrical waveguide can exhibit interesting optical properties. By exciting the free end of a MOW structure, we have shown how whispering gallery modes can be remotely excited and detected. Such remote excitation configuration can be further harnessed to detect molecular signatures in solution phase at ultra-low concentrations. Interestingly, the modes in MOW structure exhibited splitting due to symmetry breaking, as predicted by previous theoretical studies. We have also shown that by coupling a microsphere to organic waveguide, the output light characteristics with respect to input polarization changes to a quadrupolar nature. This is in contrast to conventional organic waveguide, which shows dipolar behaviour. Such coupling induced changes in the waveguiding property can be further utilized in fundamental studies of coupled-resonant systems, and the properties can be applied to micro-photonic chips and optical sensors.

Chapter 4

Plasmon Coupled Vertical Organic Nanowire

One of important question of nanophotonics is ‘how to effectively transfer information from one point to another through the channels of size much smaller than the wavelength of light?’ This question has been extensively addressed by utilizing metallic nanowire¹¹⁷. Free electrons on the surface of the metals can oscillate collectively on excitation with right frequency of electromagnetic waves²⁵. Collective oscillations of electrons coupled with electromagnetic waves are termed as surface plasmons (SPs)¹¹. Depending upon the mode of excitation there can be two types of SPs, localized or propagating. Propagating modes of nanowires were utilized for waveguiding property to transport light from one point to other. In the context of nanophotonic circuitry junctions^{33,35,36} of nanowires were utilized to control and modulate light intensities at few micrometre distances away from the excitation point.

Polarization of excitation light and polarization states of out coming light through the nanowires have rationalized the concept of building Boolean logic gates³³, optical beam splitters³⁶, quantum entanglement¹¹⁸, controllable router³⁵ and multiplexer¹¹⁹ for integrated nanophotonic circuits. All these concepts are based on linearly polarised state of light. Venture for controlling new polarisation states of light at nanoscale such as circular and radially polarised light has gained interest in recent times^{120,121}, in the concepts of building optical-magnetic recording devices.

Even though elliptically and circularly polarised light at nanoscale have been achieved through superposition of plasmon modes in metallic nanowire¹²², subwavelength circular

apertures¹²³ and L-shaped hole arrays¹²⁴, the heat generated at the operational points of system (such as edges of nanowire, sharp curvatures of L-shaped holes) due to Ohmic losses has hindered their applications^{43,44,46,47}.

Organic nanostructures have emerged to play as an important nanophotonic elements^{67,125}. These structures have composed of molecular building blocks with relatively weaker interactions, thus provide mechanical flexibility and structural tunability^{49,68,71}. Especially vertical arrangement of nanowires has been found advantageous for application as field emitters¹²⁶, nanolasers¹²⁷ and transistors⁵⁸. Utilizing organic nanostructures for controlling the polarization states of light at nanoscale is completely unexplored area. Molecules¹²⁸ are the best systems to control the polarization states since structures of the molecule can be tuned and symmetries can be controlled.

Further coupling organic nanowires with plasmons would be very advantageous because plasmons provide high density of local electric fields with modified photon density of states^{129,130}. These local fields can be utilized to tune the radiative process of building blocks of organic nanowire.

Motivated by this we coupled vertical organic nanowires with plasmonic films. In this chapter I will discuss on the photoluminescence properties of vertical nanowires. Further resolve the polarization states of emitted light.

4.1. Growth of Organic Vertical Nanowires

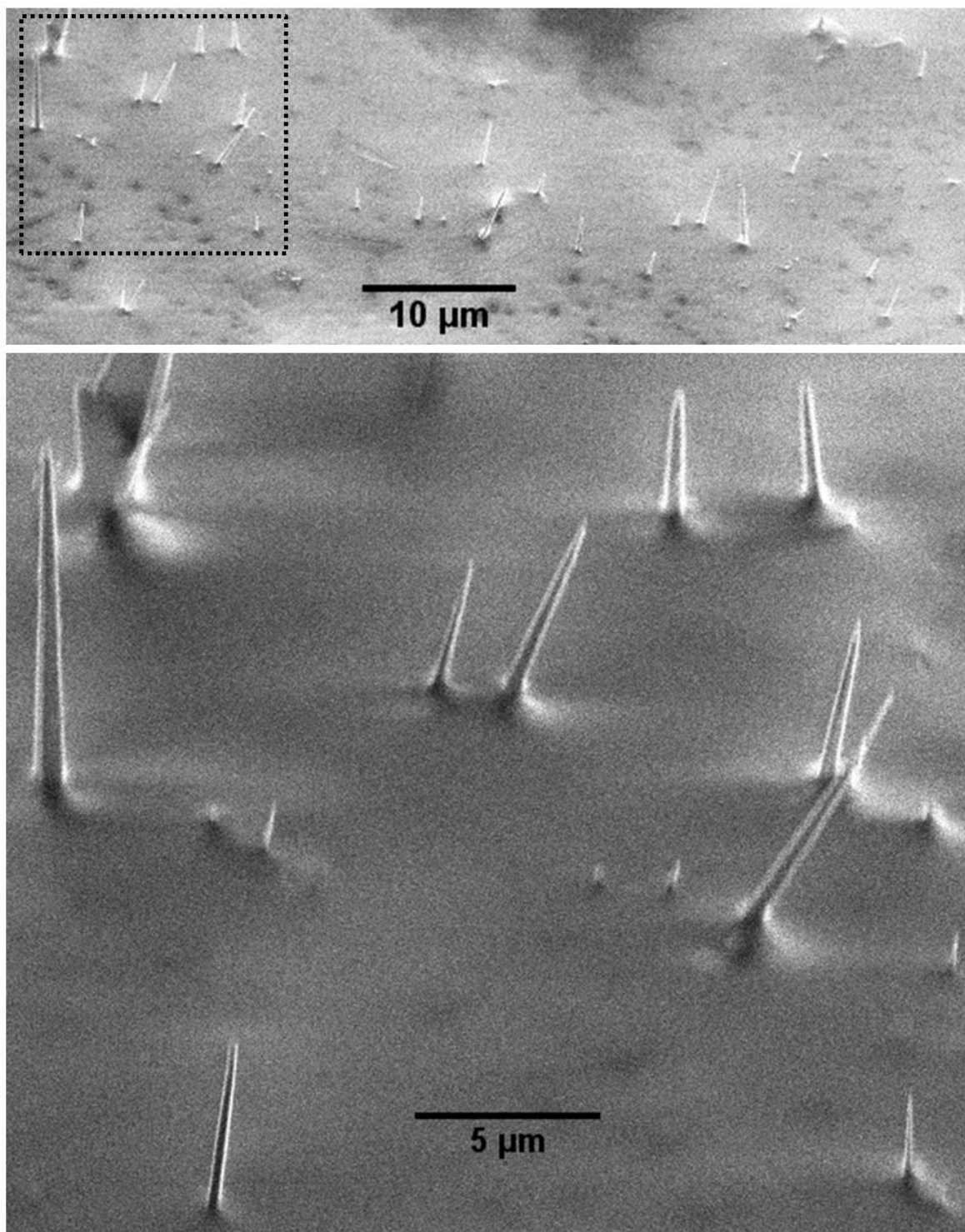


Figure 4.1: FE-SEM image of Vertical Organic Nanowires. (Top) FE - SEM image of organic nanowires grown vertically on gold metal film of thickness 100 nm, captured with 70° tilt. (Bottom) Magnified image of dotted black rectangle of top the image.

Nanowires were grown via physical deposition technique, very similar to the procedure described in [chapter 2, section 2.1](#). Instead of using a plane glass substrate for deposition of DAAQ vapour, a glass cover-slip coated with 100 nm thick metal surface (gold) was used as a substrate for condensation of DAAQ vapours. Orientation of nuclei during initial growth stage determines the growth direction of nanowires. Growth condition such as temperature also determine the dynamics of the nuclei, here evaporation temperature was fixed to 160⁰ C. A polarisable metal change the dynamics of nuclei's; C=O and -NH₂ interactions with the metal surface determine the minimal surface potential for the molecular orientation, precisely for this reason growth direction is perpendicular to the substrate and results in formation of vertical nanowires, as shown in [figure 4.1](#).

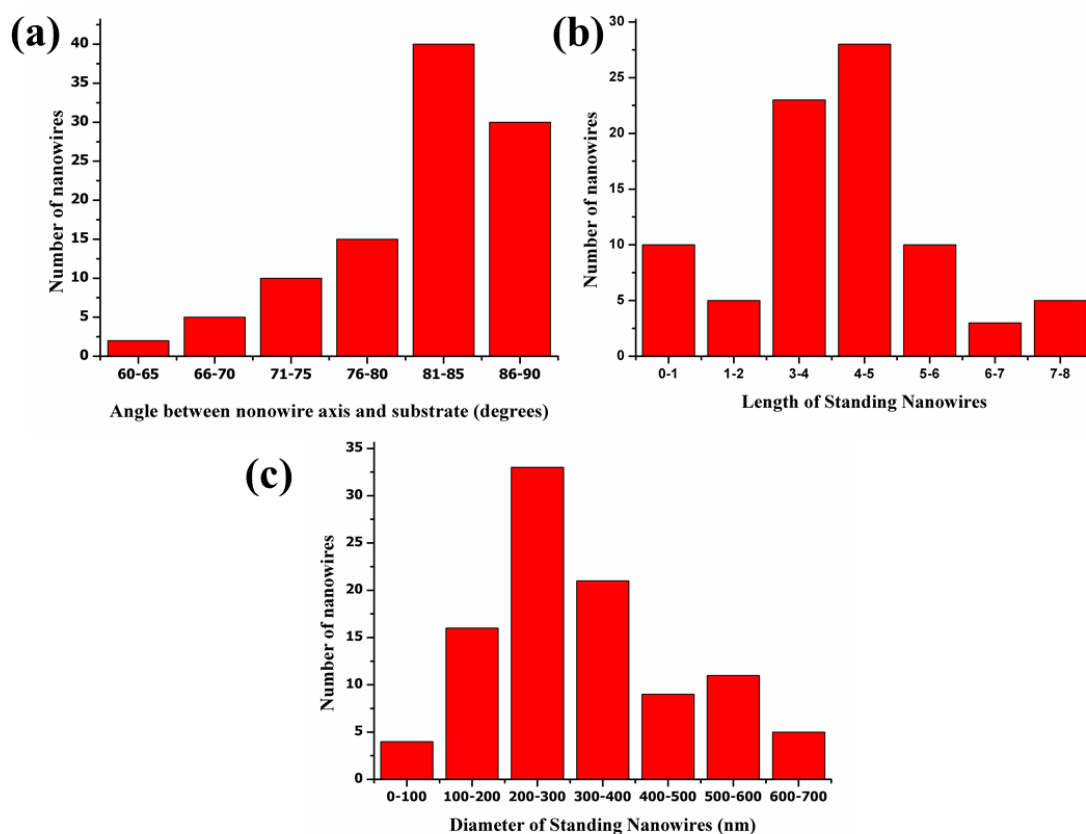


Figure 4.2: Statistical distribution of vertical nanowires. More than 100 nanowires were analysed to find the statistical distribution among the nanowires. (a) Distribution of angle between the nanowire axis and the substrate. (b) Distribution of length of nanowires. (c) Distribution of diameters of nanowire.

As we can observe in FE-SEM image ([figure 4.1](#)), there is a large distribution among the nanowires diameter, length and tilt angle. By imaging more than hundreds of nanowires through FE-SEM variation of tilt angle, length and diameter of nanowires was analysed and

histograms were plotted, see [figure 4.2](#). It is found that more than 75% of the nanowires have tilt angle between 80° - 90° , length of nanowire between $3\text{-}6\mu\text{m}$ and diameter between $200\text{-}400$ nm. Diameters were calculated via measuring full width half maxima of the nanowires. A careful observation of FE-SEM shows that these nanowires doesn't have uniform diameter, rather tapered along the length, like needles. It is hard to calculate the radius of curvature of these tips but roughly it is around ~ 50 nm. These kind of sharp tips are very important in understanding or probing single molecules.

4.2. Optical Excitation Setup

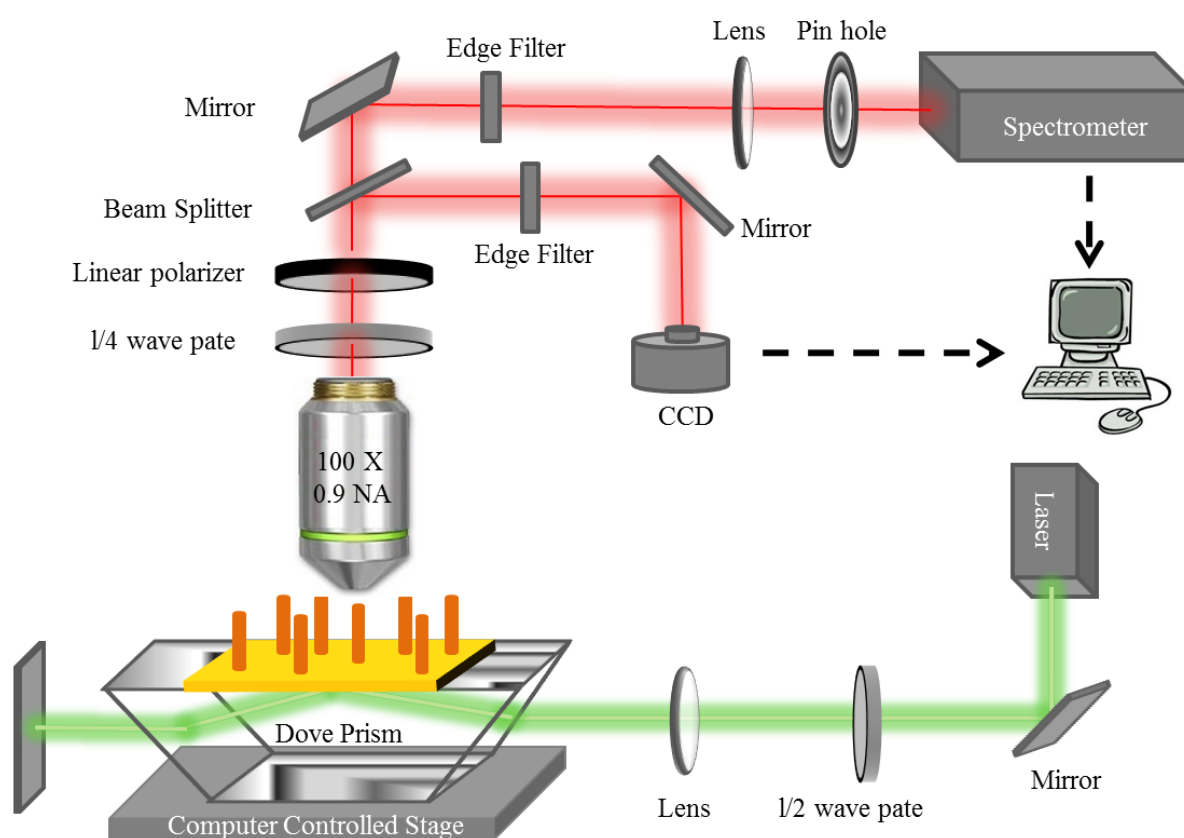


Figure 4.3: Optical excitation setup. Optical set-up of confocal Raman detection microscope coupled with Dove-prism based plasmon excitation.

[Figure 4.3](#) shows the optical schematic of the set-up used for excitation of vertical nanowire and to analyse the emission characteristics from single nanowire. We used a Dove prism (N-BK7 refractive index = 1.519), on to which a substrate used for growth of vertical nanowires was adhered through an optically matched oil. The excitation source was a 532nm, continuous-wave, frequency doubled Nd:YAG laser (power = up to 200mW) which was p-

polarized by a $\lambda/2$ plate and routed into the prism for total internal reflection by weakly focusing through a lens L (focal length = 150mm). The angle of incidence at the interface was 76.70 from the normal to the surface. The optical image and the stocks scattered signal from the vertical wires were collected via 100 \times (NA = 1) objective lens (OBL). The captured light was routed towards camera or into a high resolution, confocal Raman spectrometer (LabRam HR, 789mm focal length, pinhole size = 200 μ m). The p-polarized Gaussian excitation beam creates an elliptical projection upon total internal reflection at the sample substrate surface.

4.3. Emission Properties of Vertical Nanowires

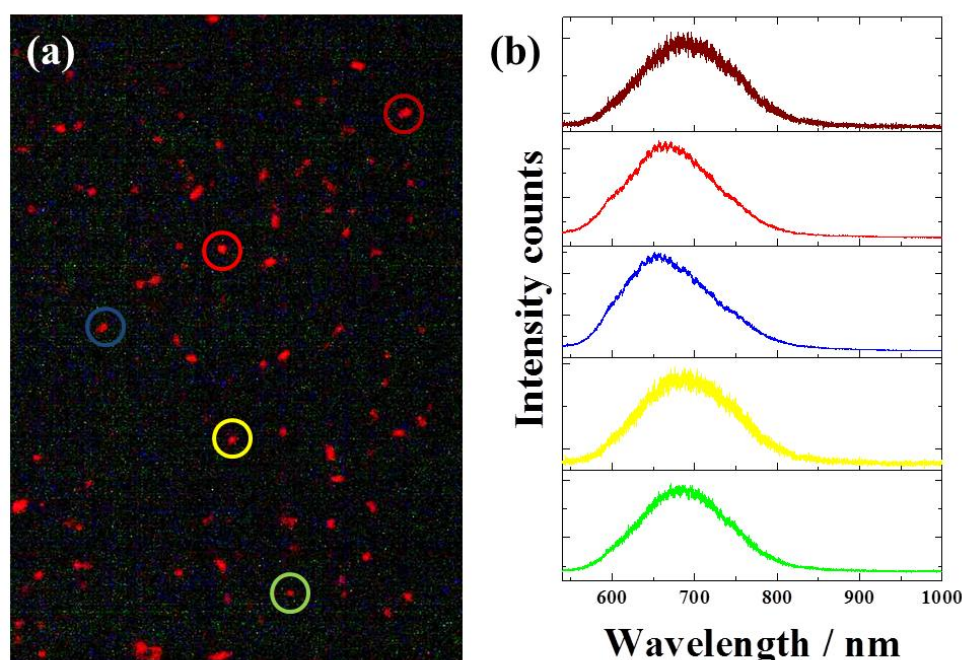


Figure 4.4: Emission from single vertical nanowires. (a) Photoluminescence image of optically well separated vertical nanowires, captured by blocking the incident laser. Each bright red spot is the emission light from a single nanowire. (b) Corresponding photoluminescence spectrum from each nanowire; particular colour of each spectrum is correlated to a PL image of nanowire represented by solid circle in (a).

Total internal reflection of incident laser at metal dielectric interface excites the surface plasmon polaritons (SPPs) on the metal film, which further excites the standing organic nanowires. The photoluminescence (PL) emission from nanowires was observed by directly routing the light into the CCD without any analyser and wave-plate in between the optical path, see [figure 4.4\(a\)](#). Rayleigh scattered from the junction of nanowires and metal surface

was filtered out by using the 532 nm edge filter. Each bright red spot in [figure 4.4\(a\)](#) corresponds to a PL emission from single vertical nanowire. It is very interesting to observe energy transfer from plasmons to excitons and further conversion of excitons to free photons. Optical element (molecules, atoms) show suppression in their PL placed on contact with metals, due to HOMO-LUMO interactions of molecules with electrons energy bands of metal.

Further, light emitter from the nanowires was routed in to the spectrometer to analyse the energy of emitted photons. Light from single nanowire was isolated by a confocal pinhole. [Figure 4.4\(b\)](#) shows the emission spectrum different nanowires, signals were accumulated for 10s. As we can see from [figure 4.4\(b\)](#), PL emission characteristic varies from a nanowire to nanowire since emission properties depends on the length and diameter of the nanowire. This kind of broad inhomogeneity would have been reflected in conventional solid state fluorescence spectrometers, in which spectrum collected will be an ensemble average of all nanowires. Precisely, for this reason understanding emission characteristics from single nanowire is very important.

4.4. Polarization States of Emitted Light

4.4.1. Probing linearly polarized state of light

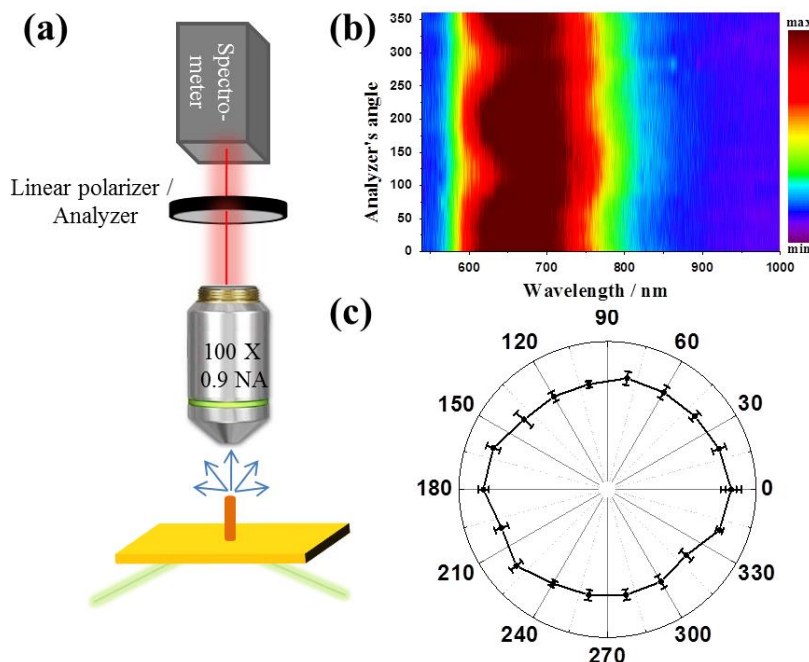


Figure 4.5: Linear polarization states of light. (a) Schematic of collection optics; light emitted from nanowire is passed through a linear polarizer (analyser) and routed into the spectrometer. (b) Waterfall image representing a series of PL spectrum as a function of analyser's angle. (c) Variation of PL intensity at 680 nm as a function of analyser's angle; data's are extracted from (b).

Resolving polarization states of emitted light is important in the context of understanding molecular dipole orientation. Motivated by this we have resolved the light emitted by the vertical nanowires in terms of their polarization states. Linearly polarized light component coming from the organic nanowires is resolved by introducing a linearly polarized analyser in a collection path (see [figure 4.5\(a\)](#)). Further the light is routed in to the spectrometer and series of spectrum was collected as a function of analyser's angle. These series of spectrum are plotted as a waterfall image, see [figure 4.5\(b\)](#). All spectrums are collected with same acquisition time of 10s. The emission intensity at 680 nm (emission maximum) was monitored as a function of analyser's angle. This intensity variation at 680 nm was plotted in polar coordinates, see [figure 4.5\(c\)](#). Intensity variation around analyser's angle found to be isotropic (irrespective of analyser's angle intensity at 680nm was found to be almost equal), giving rise to circular radiation pattern in polar coordinates. This indicates that emitted light

doesn't contain any linearly polarized light and it also implies that light coming out is either randomly polarized (unpolarized) or elliptically polarized.

4.4.2. Probing elliptically polarized states of light

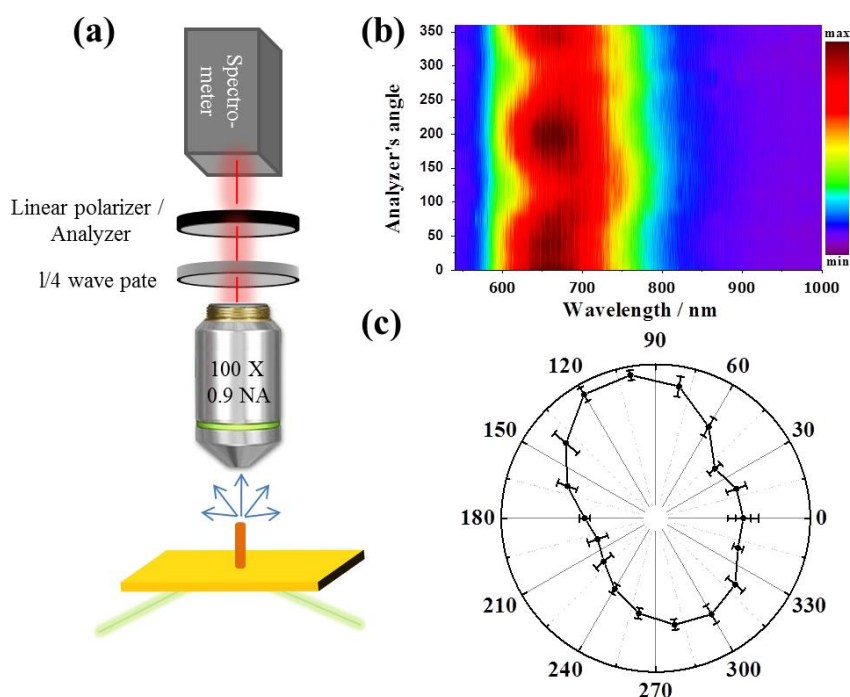


Figure 4.6: Elliptically polarization states of light. (a) Schematic of collection optics; light emitted from nanowire is passed through a $\lambda/4$ waveplate and linear polarizer (analyser), further routed into the spectrometer. (b) Waterfall image representing a series of PL spectrum as a function of analyser's angle. (c) Variation of PL intensity at 680 nm as a function of analyser's angle; data's are extracted from (b).

In order to resolve unpolarized and elliptically polarized states of emitted light from nanowire, a $\lambda/4$ waveplate was introduced in the collection pathway. Further that light is passed through a linearly polarised analysed and routed into the spectrometer, see figure 4.6(a). $\lambda/4$ waveplate converts circularly polarized light into linearly polarized light, further linearly polarized light is analysed with linearly polarizer. The series of spectrum were collection in a range of 550 nm to 1000 nm, as a function of linearly polarized analyser's angle. Very similar to previous experiments, a waterfall image was created (see [figure 4.6\(b\)](#)). The intensity variation as a function of analyser's angle showed an anisotropic distribution, see [figure 4.6\(c\)](#). A maximum intensity was observed along one axis (110

degrees) and minimum in a perpendicular axis (200 degrees), indicated a significant component of elliptically polarized states of light in an emitted light from single nanowire.

Degree of elliptically polarized (DOP) was calculated from the following equation:

$$DOP = \frac{I_{\parallel} - I_{\perp}}{I_{\parallel} + I_{\perp}} \quad \dots(4.1)$$

Where I_{\parallel} and I_{\perp} are the intensities at two complementary polarizations. The value was found to be 0.41 ± 0.03 ; At this point I would like to emphasise to the point that light emitted by the organic nanowire is a broadband spanning wavelength from 570 nm to 800 nm.

4.5. Conclusion

To conclude, we have successfully grown the organic nanowires perpendicular to the metallic substrate. Nanowires are tapered at the tips with high degree of radius of curvature. A linearly polarized light was used to excite these nanowires via evanescent field. Energy transfer from plasmons of metal film to the excitons of the nanowires was understood and emitted light is a broadband light source at subwavelength scales. Further we resolved the polarization states of light emitted from single vertical nanowires and found that emitted light contains relatively high degree of elliptically polarized light, which is the central result of this chapter.

Chapter 5

Future Direction

We have understood the properties of organic nanowires and perturbation of their properties on coupling with dielectric microsphere or plasmonic films in this thesis. Further I am interested in studying interaction of organic structures (which are basically small cluster of molecules) with plasmonic cavities and plasmonic tips. Here I will discuss of these ideas in detail.

5.1. Excitons coupled with periodic plasmonic tips

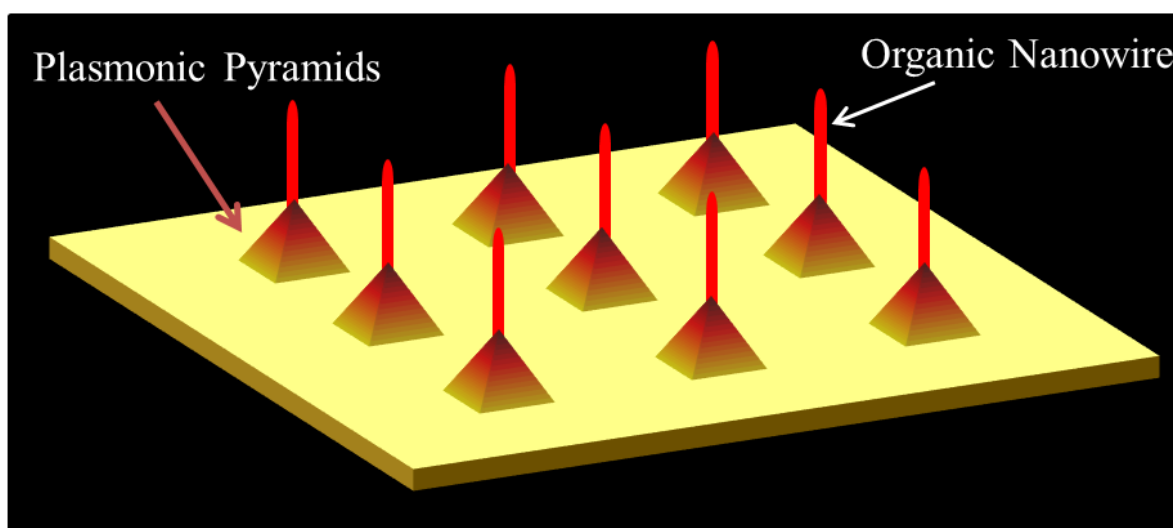


Figure 5.1: Exciton – plasmon coupling & periodic architecture. Schematic illustration of periodic plasmonic tips coupled with organic nanowires.

In [chapter 4](#) we had discussed on the emission polarisation states of light by organic being perturbed on coupling with the plasmonic films. There it was propagating surface plasmon polaritons (SPPs) being interacting with the local excitons of organic nanowire. Here, the question that I am trying to address is ‘how do excitons interact with highly localized electric fields? In order to address to this I have formulated a prototype (see [figure 5.1](#)). [Figure 5.1](#), shows schematic of periodic plasmonic pyramids and each pyramids are coupled with organic nanowire. These pyramids are known to show effects similar to lightning rod effect. On

excitation pyramids confines the electric into their tips, the electric field enhancements at the tips can as high as 10^9 . Molecules of nanowires sitting in the vicinity such high local fields, prone to exhibit modified radiation patterns and excited state lifetimes get perturbed. Further due to periodicity in the arrangement of nanowires, new resonance can arise.

We have already made some progress in addressing these questions by fabricating periodic subwavelength holes and disc, see [figure 5.2](#). These structures were fabricated with using template stripping technique, in which a complementary structure written on silicon wafer is transfer into glass, by depositing thin layer of metal on to the silicon wafer and then epoxy glue was used to strip out the metal structure. Now the plan is to selective grow organic nanowires on metallic disc or on plasmonic holes.

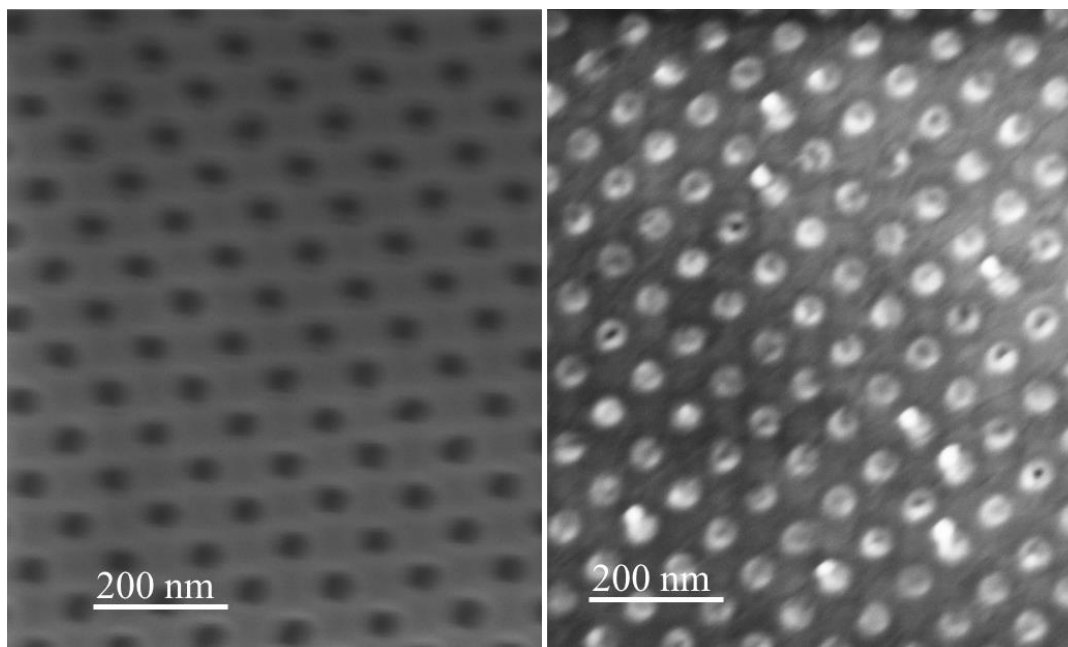


Figure 5.2: Periodic nanoplasmonic architectures. (Left) FE-SEM image of periodic nanoholes on thin gold metal film of 100 nm. (Right) FE-SEM image of gold nanodisks. Both the structures are fabricated via template stripping technique.

5.2. Strong Coupling between plasmons and excitons

Relatively long term problem that I am interested in studying is ‘strong coupling’ between organic semiconductors and plasmonic cavities. The interaction of optical elements (such as molecules, quantum dots, nitrogen vacancies) with surface plasmon can be distinguished in two coupling regimes. In the weak coupling regime, damping of either resonance dominates

over coupling and the interaction only modifies the radiative decay rate of the exciton state (Purcell effect) and its angular radiation pattern. Perturbation can be understood through Fermi golden rule and emission rates can be estimated. Whereas, in the strong coupling regime, the states of the surface plasmons-exciton system are coherent super positions of both types of excitations and one can't distinguish the acceptor and donor. This give rise to interesting optical properties such as electromagnetic transparency dips in transmittance and reflectivity spectrums.

So I am interested in construction of nanocavity of dimensions down to a single nanometre, together with the encapsulation of organic semiconductors. The aim will be to look at the coupling between the electronic states in the semiconductors with the plasmons in the nanocavity. This will lead to the potential for optical switches operating on ultralow power thresholds. The research will involve fabrication, building new optical spectroscopy tools, analysis and simple theories to explain the results and the device performance.

Appendix

Mie theory

Mie theory is concerned with the description of the scattering properties of a sphere (dielectric or metallic) of arbitrary size. The theory provides exact solution to the electromagnetic problem, but theory as such is not user friendly since it make use of special functions such as spherical harmonics and spherical Bessel functions.

Consider a homogeneous, isotropic and non-magnetic material whose optical properties are characterized by frequency dependent dielectric function $\epsilon(\omega)$. Finding divergence-less electric field solution of the Helmholtz equation is required in solving EM problems related to scattering by dielectric spheres.

$$\Delta^2 E + k^2 E = 0 \text{ and } \nabla \cdot E = 0 \quad \dots(\text{A. 1})$$

where the wave vector is given by:

$$k^2 = \frac{\omega^2}{c^2} \epsilon(\omega) \quad \dots(\text{A. 2})$$

Finding the divergence-less solutions of the vectorial wave equation is not difficult; the tricky part is to find a solution that satisfies boundary conditions at all interfaces.

Here will calculate the scattering coefficients for a dielectric sphere by utilizing spherical coordinates. The divergence-less solution of vector wave equations in spherical coordinates can be written as follows:

$$E(r) = E_0 \sum_{n=0}^{\infty} \sum_{m=-n}^{m=n} a_{nm} M_{nm}^{(i)}(k, r) + b_{nm} N_{nm}^{(i)}(k, r) \quad \dots(\text{A. 3})$$

Where the vectors $M_{nm}^{(i)}(k, r)$ and $N_{nm}^{(i)}(k, r)$ are called vector spherical harmonics or multipole fields. Physically n can be interpreted as the total angular momentum, while m is the projection of this momentum along z-axis.

We have calculated scattering efficiencies for microspheres of 5 μm in Mie regime of $20 < x < 26$, where x is a size parameter, $x = ka$ (a is the radius of microsphere; $k = \frac{2\pi}{\lambda}$ is the wave

number). The efficiencies Q_i for the interaction of radiation with sphere of radius a and cross-section σ_i , is given by

$$Q_i = \frac{\sigma_i}{2\pi a^2} \quad \dots(\text{A. 4})$$

the extension efficiency Q_{ext} which is sum of Q_{scatt} (scattering) and Q_{abs} (absorption), which is also called as forward scattering is given by

$$Q_{ext} = \frac{2}{(ka)^2} \sum_{n=1}^{\infty} (2n+1) \text{Re}(a_n + b_n) \quad \dots(\text{A. 5})$$

Where k is the wave number; a_n and b_n are mie coefficients to compute amplitude of scattering fields, these coefficients involve spherical Bessel functions of higher order. The complete expression for a_n and b_n is given by

$$a_n = \bar{m}\psi_n(\bar{m}x)\psi'_n(x) - \psi_n(x)\psi'_n(\bar{m}x) / A \quad \dots(\text{A. 6})$$

$$b_n = \psi_n(\bar{m}x)\psi'_n(x) - \bar{m}\psi_n(x)\psi'_n(\bar{m}x) / B \quad \dots(\text{A. 7})$$

where denominators A and B are given by

$$A = \left(\frac{D_n(\bar{m}x)}{\bar{m}} + \frac{n}{x} \right) (\xi_n(x) - \xi_{n-1}(x)) \quad \dots(\text{A. 8})$$

$$B = \left(\bar{m}D_n(\bar{m}x) + \frac{n}{x} \right) (\xi_n(x) - \xi_{n-1}(x)) \quad \dots(\text{A. 9})$$

ψ_n and ξ_n are the Riccati Bessel functions defined as $\psi_n(r) = rj_n(r)$ and $\xi_n(r) = rh_n(r)$, primes denote derivatives with respect to the argument and D_n is the logarithmic derivative.

a_n and b_n are computed for $n = 1 \dots N$ ($N = x + 4x^{1/3} + 2$) from size parameter x and index of refraction $m = 1.457$ using recursion relation for spherical Bessel functions. Resonance occurs when the internal fields are very high, i.e. when a_n and b_n parameter is large, which will occur when the denominator A or B is zero. When A is zero, a_n parameter dominates, resonances corresponding this are assigned as TM-mode. Similarly when B is zero, b_n will dominate and resonances corresponding to this are assigned as TE-mode.

Characterization of WGMs

WGMs are characterized by two polarization (TE and TM) and 3 mode numbers (n, l, m) which are called as radial, angular and azimuthal quantum numbers. The mode number n corresponds to half the number of field maxima's along the great periphery of the sphere and mode number l is equal to number of field maxima in the direction along the radius of sphere.

For perfect spheres having spherical / azimuthal symmetry the mode number m (values from $-n$ to $+n$) corresponding to clock-wise (CW) or counter clock-wise (CCW) directional modes are degenerate.

References:

- 1 Lakowicz, J. R. *Principles of Fluorescence Spectroscopy*. (Springer, 2006).
- 2 Jackson, J. D. *Classical electrodynamics*. (Wiley, 1975).
- 3 Griffiths, D. J. *Introduction to Electrodynamics*. (Pearson Education, Limited, 2012).
- 4 Hecht, E. G. A. R. *Optics*. (Addison-Wesley, 2002).
- 5 Fenna, R. E. & Matthews, B. W. Chlorophyll arrangement in a bacteriochlorophyll protein from *Chlorobium limicola*. *Nature* **258**, 573-577 (1975).
- 6 Engel, G. S. *et al.* Evidence for wavelike energy transfer through quantum coherence in photosynthetic systems. *Nature* **446**, 782-786, (2007).
- 7 Schaefer, H. E. *Nanoscience*, 2010).
- 8 Huang, K. *Statistical mechanics*. (Wiley, 1987).
- 9 Cohen-Tannoudji, C. D. B. L. F. *Quantum mechanics*. (Wiley, 1977).
- 10 Shankar, R. *Principles of quantum mechanics*. (Plenum Press, 1980).
- 11 Novotny, L. H. B. *Principles of nano-optics*. (Cambridge University Press, 2006).
- 12 Vahala, K. J. Optical microcavities. *Nature* **424**, 839-846 (2003).
- 13 Haroche, S. & Kleppner, D. Cavity quantum electrodynamics. *Phys. Today* **42**, 24-30 (1989).
- 14 Ward, J. & Benson, O. WGM microresonators: sensing, lasing and fundamental optics with microspheres. *Laser & Photonics Reviews* **5**, 553-570, doi:10.1002/lpor.201000025 (2011).
- 15 Thompson, R. J., Rempe, G. & Kimble, H. J. Observation of normal-mode splitting for an atom in an optical cavity. *Physical Review Letters* **68**, 1132-1135 (1992).
- 16 Purcell, E. M. 681 (Phys. Rev).
- 17 Armani, D. K., Kippenberg, T. J., Spillane, S. M. & Vahala, K. J. Ultra-high-Q toroid microcavity on a chip. *Nature* **421**, 925-928 (2003).
- 18 Chiasera, A. *et al.* Spherical whispering-gallery-mode microresonators. *Laser & Photonics Reviews* **4**, 457-482, doi:10.1002/lpor.200910016 (2010).
- 19 Bohren, C. F. H. D. R. *Absorption and scattering of light by small particles*. (Wiley, 1983).
- 20 Jenkins, F. A. W. H. E. *Fundamentals of optics*. (McGraw-Hill, 1957).
- 21 Malvino, A. P. L. D. P. *Digital principles and applications*. (Gregg Division, McGraw-Hill, 1981).
- 22 Beyond the diffraction limit. *Nat Photon* **3**, 361-361 (2009).
- 23 Kawata, S., Inouye, Y. & Verma, P. Plasmonics for near-field nano-imaging and superlensing. *Nat Photon* **3**, 388-394 (2009).
- 24 HongáCui, Q. & ShengáZhao, Y. Photonic applications of one-dimensional organic single-crystalline nanostructures: optical waveguides and optically pumped lasers. *Journal of Materials Chemistry* **22**, 4136-4140 (2012).
- 25 Barnes, W. L., Dereux, A. & Ebbesen, T. W. Surface plasmon subwavelength optics. *Nature* **424**, 824-830, doi:10.1038/nature01937 (2003).
- 26 Maier, S. A. *Plasmonics: Fundamentals and Applications*. (Springer, 2007).
- 27 Anker, J. N. *et al.* Biosensing with plasmonic nanosensors. *Nature Materials* **7**, 442-453 (2008).
- 28 Sanders, A. W. *et al.* Observation of plasmon propagation, redirection, and fan-out in silver nanowires. *Nano Letters* **6**, 1822-1826 (2006).
- 29 Kik, P. G. & Brongersma, M. L. in Vol. 131, Springer Series in Optical Sciences 1-9 (Springer, Dordrecht, 2007).
- 30 Sun, Y., Yin, Y., Mayers, B. T., Herricks, T. & Xia, Y. Uniform Silver Nanowires Synthesis by Reducing AgNO₃ with Ethylene Glycol in the Presence of Seeds and Poly(Vinyl Pyrrolidone). *Chemistry of Materials* **14**, 4736-4745, doi:10.1021/cm020587b (2002).
- 31 Kim, F., Sohn, K., Wu, J. & Huang, J. Chemical Synthesis of Gold Nanowires in Acidic Solutions. *Journal of the American Chemical Society* **130**, 14442-14443, doi:10.1021/ja806759v (2008).
- 32 Ma, Y. *et al.* Direct measurement of propagation losses in silver nanowires. *Opt. Lett.* **35**, 1160-1162 (2010).
- 33 Wei, H., Wang, Z., Tian, X., Kall, M. & Xu, H. Cascaded logic gates in nanophotonic plasmon networks. *Nat. Comm.* **2**, 387 (2011).
- 34 Dittlacher, H. *et al.* Silver nanowires as surface plasmon resonators. *Physical Review Letters* **95**, 1-4 (2005).
- 35 Fang, Y. *et al.* Branched silver nanowires as controllable plasmon routers. *Nano Letters* **10**, 1950-1954 (2010).

- 36 Singh, D., Raghuwanshi, M. & Pavan Kumar, G. V. Propagation of light in serially coupled plasmonic nanowire dimer: Geometry dependence and polarization control. *Applied Physics Letters* **101**, (2012).
- 37 Chikkaraddy, R., Singh, D. & Pavan Kumar, G. V. Plasmon assisted light propagation and Raman scattering hot-spot in end-to-end coupled silver nanowire pairs. *Applied Physics Letters* **100**, (2012).
- 38 Seung, J. L., Jeong, M. B. & Moskovits, M. Polarization-dependent surface-enhanced raman scattering from a silver-nanoparticle-decorated single silver nanowire. *Nano Letters* **8**, 3244-3247 (2008).
- 39 Baik, J. M., Lee, S. J. & Moskovits, M. Polarized surface-enhanced Raman spectroscopy from molecules adsorbed in nano-gaps produced by electromigration in silver nanowires. *Nano Letters* **9**, 672-676 (2009).
- 40 Fang, Y., Wei, H., Hao, F., Nordlander, P. & Xu, H. Remote-excitation surface-enhanced raman scattering using propagating ag nanowire plasmons. *Nano Letters* **9**, 2049-2053 (2009).
- 41 Shegai, T., Huang, Y., Xu, H. & Käll, M. Coloring fluorescence emission with silver nanowires. *Applied Physics Letters* **96**, (2010).
- 42 Gramotnev, D. K. & Bozhevolnyi, S. I. Plasmonics beyond the diffraction limit. *Nat Photon* **4**, 83-91 (2010).
- 43 Khurgin, J. B. & Sun, G. In search of the elusive lossless metal. *Applied Physics Letters* **96**, (2010).
- 44 West, P. R. *et al.* Searching for better plasmonic materials. *Laser & Photonics Reviews* **4**, 795-808, (2010).
- 45 Stockman, M. I. Criterion for Negative Refraction with Low Optical Losses from a Fundamental Principle of Causality. *Physical Review Letters* **98**, 177404 (2007).
- 46 Dimmock, J. Losses in left-handed materials. *Opt. Express* **11**, 2397-2402, (2003).
- 47 Markoš, P., Rousochatzakis, I. & Soukoulis, C. M. Transmission losses in left-handed materials. *Physical Review E* **66**, 045601 (2002).
- 48 Clark, J. & Lanzani, G. Organic photonics for communications. *Nat Photon* **4**, 438-446 (2010).
- 49 Zheng, J. Y. *et al.* Wire-on-wire growth of fluorescent organic heterojunctions. *Journal of the American Chemical Society* **134**, 2880-2883 (2012).
- 50 Zhao, Y. S. *et al.* Optical waveguide based on crystalline organic microtubes and microrods. *Angewandte Chemie* **120**, 7411-7415 (2008).
- 51 Takazawa, K., Kitahama, Y., Kimura, Y. & Kido, G. Optical waveguide self-assembled from organic dye molecules in solution. *Nano Letters* **5**, 1293-1296 (2005).
- 52 Kaino, T. Waveguide fabrication using organic nonlinear optical materials. *Journal of Optics A: Pure and Applied Optics* **2**, R1 (2000).
- 53 Chandrasekar, R. Organic Photonics: Prospective nano/micro scale passive organic optical wave guides obtained from pi-conjugated ligand molecules. *Physical Chemistry Chemical Physics* (2014).
- 54 Kozlov, V. G., Bulovic, V., Burrows, P. E. & Forrest, S. R. Laser action in organic semiconductor waveguide and double-heterostructure devices. *Nature* **389**, 362-364 (1997).
- 55 Takazawa, K., Inoue, J.-i., Mitsuishi, K. & Takamasu, T. Fraction of a millimeter propagation of exciton polaritons in photoexcited nanofibers of organic dye. *Physical review letters* **105**, 067401 (2010).
- 56 Zhang, C., Zhao, Y. S. & Yao, J. Optical waveguides at micro/nanoscale based on functional small organic molecules. *Physical Chemistry Chemical Physics* **13**, 9060-9073 (2011).
- 57 Penner, T. L., Motschmann, H. R., Armstrong, N. J., Ezenyilimba, M. C. & Williams, D. J. Efficient phase-matched second-harmonic generation of blue light in an organic waveguide. *Nature* **367**, 49-51 (1994).
- 58 Briseno, A. L., Mannsfeld, S. C., Jenekhe, S. A., Bao, Z. & Xia, Y. Introducing organic nanowire transistors. *Materials Today* **11**, 38-47 (2008).
- 59 Ellenbogen, T., Steinvurzel, P. & Crozier, K. B. Strong coupling between excitons in J-aggregates and waveguide modes in thin polymer films. *Applied Physics Letters* **98**, (2011).
- 60 Ulbrich, R. G. & Fehrenbach, G. W. Polariton Wave Packet Propagation in the Exciton Resonance of a Semiconductor. *Physical Review Letters* **43**, 963-966 (1979).
- 61 Yan, Y. & Zhao, Y. S. Exciton Polaritons in 1D Organic Nanocrystals. *Advanced Functional Materials* **22**, 1330-1332, doi:10.1002/adfm.201102173 (2012).
- 62 Lal, S., Link, S. & Halas, N. J. Nano-optics from sensing to waveguiding. *Nat Photon* **1**, 641-648 (2007).
- 63 Jenkins, A. The road to nanophotonics. *Nat Photon* **2**, 258-260 (2008).
- 64 Tong, L. *et al.* Subwavelength-diameter silica wires for low-loss optical wave guiding. *Nature* **426**, 816-819 (2003).
- 65 Ma, H., Jen, A. K. Y. & Dalton, L. R. Polymer-Based Optical Waveguides: Materials, Processing, and Devices. *Advanced Materials* **14**, 1339-1365, (2002).

- 66 Balzer, F., Bordo, V. G., Simonsen, A. C. & Rubahn, H.-G. Isolated hexaphenyl nanofibers as optical waveguides. *Applied Physics Letters* **82**, 10-12, (2003).
- 67 Barrelet, C. J., Greytak, A. B. & Lieber, C. M. Nanowire Photonic Circuit Elements. *Nano Letters* **4**, (2004).
- 68 Zhao, Y. S. *et al.* Low-Dimensional Nanomaterials Based on Small Organic Molecules: Preparation and Optoelectronic Properties. *Advanced Materials* **20**, 2859-2876, (2008).
- 69 Zhao, Y. S. *et al.* Construction and Optoelectronic Properties of Organic One-Dimensional Nanostructures. *Accounts of Chemical Research* **43**, 409-418, (2009).
- 70 Bi, H. *et al.* Fac-Alq₃ and Mer-Alq₃ Nano/Microcrystals with Different Emission and Charge-Transporting Properties. *Advanced Materials* **22**, 1631-1634, (2010).
- 71 Zang, L., Che, Y. & Moore, J. S. One-Dimensional Self-Assembly of Planar π -Conjugated Molecules: Adaptable Building Blocks for Organic Nanodevices. *Accounts of Chemical Research* **41**, 1596-1608, (2008).
- 72 Zhao, Y. S. *et al.* Photoluminescence and Electroluminescence from Tris(8-hydroxyquinoline)aluminum Nanowires Prepared by Adsorbent-Assisted Physical Vapor Deposition. *Advanced Functional Materials* **16**, 1985-1991, (2006).
- 73 Jang, J. & Oh, J. H. Facile Fabrication of Photochromic Dye-Conducting Polymer Core-Shell Nanomaterials and Their Photoluminescence. *Advanced Materials* **15**, 977-980, (2003).
- 74 Zhao, Y. S., Fu, H., Hu, F., Peng, A. D. & Yao, J. Multicolor Emission from Ordered Assemblies of Organic 1D Nanomaterials. *Advanced Materials* **19**, 3554-3558, (2007).
- 75 Che, Y., Yang, X., Loser, S. & Zang, L. Expedient Vapor Probing of Organic Amines Using Fluorescent Nanofibers Fabricated from an n-Type Organic Semiconductor. *Nano Letters* **8**, 2219-2223, (2008).
- 76 Li, X., Gao, N., Xu, Y., Li, F. & Ma, Y. Self-cavity laser oscillations with very low threshold from a symmetric organic crystal waveguide. *Applied Physics Letters* **101**, (2012).
- 77 Zhao, Y. S., Wu, J. & Huang, J. Vertical organic nanowire arrays: Controlled synthesis and chemical sensors. *Journal of the American Chemical Society* **131**, 3158-3159 (2009).
- 78 Zhao, Y. S., Zhan, P., Kim, J., Sun, C. & Huang, J. Patterned growth of vertically aligned organic nanowire waveguide arrays. *ACS nano* **4**, 1630-1636 (2010).
- 79 Stutzman, W. L. T. G. A. *Antenna theory and design*. (Wiley, 1981).
- 80 Qian, Y., Deal, W., Kaneda, N. & Itoh, T. Microstrip-fed quasi-Yagi antenna with broadband characteristics. *Electronics Letters* **34**, 2194-2196 (1998).
- 81 Bharadwaj, P., Deutsch, B. & Novotny, L. Optical antennas. *Advances in Optics and Photonics* **1**, 438-483 (2009).
- 82 Chung, T., Lee, S.-Y., Song, E. Y., Chun, H. & Lee, B. Plasmonic nanostructures for nano-scale bio-sensing. *Sensors* **11**, 10907-10929 (2011).
- 83 Grillet, N. *et al.* Plasmon coupling in silver nanocube dimers: Resonance splitting induced by edge rounding. *ACS nano* **5**, 9450-9462 (2011).
- 84 Kinkhabwala, A. *et al.* Large single-molecule fluorescence enhancements produced by a bowtie nanoantenna. *Nature Photonics* **3**, 654-657 (2009).
- 85 Dhawan, A., Gerhold, M. D. & Muth, J. F. Plasmonic structures based on subwavelength apertures for chemical and biological sensing applications. *Sensors Journal, IEEE* **8**, 942-950 (2008).
- 86 Kosako, T., Kadoya, Y. & Hofmann, H. F. Directional control of light by a nano-optical Yagi-Uda antenna. *Nature Photonics* **4**, 312-315 (2010).
- 87 Dorfmüller, J. *et al.* Plasmonic nanowire antennas: experiment, simulation, and theory. *Nano letters* **10**, 3596-3603 (2010).
- 88 Lal, S., Link, S. & Halas, N. J. Nano-optics from sensing to waveguiding. *Nature Photonics* **1**, 641-648 (2007).
- 89 Jenkins, A. The road to nanophotonics. *Nature Photonics* **2**, 258-260 (2008).
- 90 Penner, T. L., Motschmann, H. R., Armstrong, N. J., Ezenyilimba, M. C. & Williams, D. J. Efficient phase-matched second-harmonic generation of blue light in an organic waveguide. *Nature* **367**, 49-50 (1994).
- 91 Kozlov, V. G., Bulovič, V., Burrows, P. E. & Forrest, S. R. Laser action, in organic semiconductor waveguide and double-heterostructure devices. *Nature* **389**, 362-364 (1997).
- 92 Zhao, Y. S. *et al.* Optical waveguide based on crystalline organic microtubes and microrods. *Angewandte Chemie - International Edition* **47**, 7301-7305 (2008).
- 93 Clark, J. & Lanzani, G. Organic photonics for communications. *Nature Photonics* **4**, 438-446 (2010).
- 94 Quan, F. Green photonics. *Journal of Optics* **14** (2012).
- 95 Yang, F., Sambles, J. R. & Bradberry, G. W. Long-range coupled surface exciton polaritons. *Physical Review Letters* **64**, 559-562 (1990).

- 96 Van Vugt, L. K. *et al.* Exciton polaritons confined in a ZnO nanowire cavity. *Physical Review Letters* **97** (2006).
- 97 Kaino, T. Waveguide fabrication using organic nonlinear optical materials. *Journal of Optics A: Pure and Applied Optics* **2**, R1-R7 (2000).
- 98 Li, X., Gao, N., Xu, Y., Li, F. & Ma, Y. Self-cavity laser oscillations with very low threshold from a symmetric organic crystal waveguide. *Applied Physics Letters* **101** (2012).
- 99 Yan, Y., Zhang, C., Zheng, J. Y., Yao, J. & Zhao, Y. S. Optical modulation based on direct photon-plasmon coupling in organic/metal nanowire heterojunctions. *Advanced Materials* **24**, 5681-5686 (2012).
- 100 Righini, G. C. *et al.* Whispering gallery mode microresonators: Fundamentals and applications. *Riv Nuovo Cimento* **34**, 435-488, (2011).
- 101 Dutta Gupta, S. & Agarwal, G. S. Strong coupling cavity physics in microspheres with whispering gallery modes. *Optics Communications* **115**, 597-605 (1995).
- 102 Dutta Gupta, S. & Agarwal, G. S. Quantum optics and electrodynamics in microstructures. *Frontiers in Atomic, Molecular and Optical Physics* **3**, 301-330 (2003).
- 103 Chiasera, A. *et al.* Spherical whispering-gallery-mode microresonators. *Laser and Photonics Reviews* **4**, 457-482 (2010).
- 104 Ward, J. & Benson, O. WGM microresonators: Sensing, lasing and fundamental optics with microspheres. *Laser and Photonics Reviews* **5**, 553-570 (2011).
- 105 Vollmer, F. & Arnold, S. Whispering-gallery-mode biosensing: label-free detection down to single molecules. *Nat Meth* **5**, 591-596 (2008).
- 106 Vollmer, F., Arnold, S. & Keng, D. Single virus detection from the reactive shift of a whispering-gallery mode. *Proceedings of the National Academy of Sciences of the United States of America* **105**, 20701-20704 (2008).
- 107 Santiago-Cordoba, M. A., Boriskina, S. V., Vollmer, F. & Demirel, M. C. Nanoparticle-based protein detection by optical shift of a resonant microcavity. *Applied Physics Letters* **99**, -, (2011).
- 108 Ta, V. D., Chen, R. & Sun, H. D. Tuning whispering gallery mode lasing from self-assembled polymer droplets. *Scientific Reports* **3** (2013).
- 109 Dominguez-Juarez, J. L., Kozyreff, G. & Martorell, J. Whispering gallery microresonators for second harmonic light generation from a low number of small molecules. *Nat Commun* **2**, 254 (2011).
- 110 Kozyreff, G., Dominguez-Juarez, J. L. & Martorell, J. Nonlinear optics in spheres: from second harmonic scattering to quasi-phase matched generation in whispering gallery modes. *Laser & Photonics Reviews* **5**, 737-749, (2011).
- 111 Bilici, T., Isci, S., Kurt, A. & Serpengözel, A. Microsphere-Based Channel Dropping Filter With an Integrated Photodetector. *IEEE Photonics Technology Letters* **16**, 476-478 (2004).
- 112 Dong, C. H. *et al.* Fabrication of high-Q polydimethylsiloxane optical microspheres for thermal sensing. *Applied Physics Letters* **94** (2009).
- 113 Aoki, T. *et al.* Observation of strong coupling between one atom and a monolithic microresonator. *Nature* **443**, 671-674 (2006).
- 114 Klinner, J., Lindholdt, M., Nagorny, B. & Hemmerich, A. Normal mode splitting and mechanical effects of an optical lattice in a ring cavity. *Physical Review Letters* **96** (2006).
- 115 Rao, V. S. C. M. & Gupta, S. D. Broken azimuthal degeneracy with whispering gallery modes of microspheres. *Journal of Optics A: Pure and Applied Optics* **7**, 279-285 (2005).
- 116 Weiss, D. S. *et al.* Splitting of high-Q Mie modes induced by light backscattering in silica microspheres. *Opt. Lett.* **20**, 1835-1837 (1995).
- 117 Lal, S., Hafner, J. H., Halas, N. J., Link, S. & Nordlander, P. Noble Metal Nanowires: From Plasmon Waveguides to Passive and Active Devices. *Accounts of Chemical Research* **45**, 1887-1895, doi:10.1021/ar300133j (2012).
- 118 Chen, G.-Y., Lambert, N., Chou, C.-H., Chen, Y.-N. & Nori, F. Surface plasmons in a metal nanowire coupled to colloidal quantum dots: scattering properties and quantum entanglement. *Physical Review B* **84**, 045310 (2011).
- 119 Imre, A., Vlasko-Vlasov, V. K., Pearson, J., Hiller, J. M. & Welp, U. Multiplexing surface plasmon polaritons on nanowires. *Applied Physics Letters* **91**, (2007).
- 120 Ögüt, E. & Şendur, K. Tuning the polarization states of optical spots at the nanoscale on the Poincaré sphere using a plasmonic nanoantenna. *Appl. Phys. A* **103**, 855-858, (2011).
- 121 Biagioni, P. *et al.* 79220C-79220C-79225.
- 122 Zhang, S. *et al.* Chiral surface plasmon polaritons on metallic nanowires. *Physical review letters* **107**, 096801 (2011).
- 123 Drezet, A., Genet, C. & Ebbesen, T. W. Miniature Plasmonic Wave Plates. *Physical Review Letters* **101**, 043902 (2008).

- 124 Li, T. *et al.* Manipulating optical rotation in extraordinary transmission by hybrid plasmonic excitations. *Applied Physics Letters* **93**, (2008).
- 125 Takazawa, K., Inoue, J. i., Mitsuishi, K. & Kuroda, T. Ultracompact Asymmetric Mach–Zehnder Interferometers with High Visibility Constructed from Exciton Polariton Waveguides of Organic Dye Nanofibers. *Advanced Functional Materials* **23**, 839-845 (2012).
- 126 Huang, K.-J., Hsiao, Y.-S. & Whang, W.-T. Low-temperature formation of self-assembled 1,5-diaminoanthraquinone nanofibers: Substrate effects and field emission characteristics. *Organic Electronics* **12**, 686-693, (2011).
- 127 Zhang, C. *et al.* Two-photon pumped lasing in single-crystal organic nanowire exciton polariton resonators. *Journal of the American Chemical Society* **133**, 7276-7279 (2011).
- 128 Lieb, M. A., Zavislan, J. M. & Novotny, L. Single-molecule orientations determined by direct emission pattern imaging. *J. Opt. Soc. Am. B* **21**, 1210-1215, (2004).
- 129 Dionne, J. A. Nanoplasmonics: Plasmons rock in metal bands. *Nat Mater* **12**, 380-381, (2013).
- 130 Sviatlana, V. *et al.* Tailoring and imaging the plasmonic local density of states in crystalline nanoprisms. *Nature Materials* **12**, (2013).